Single-cell lineage tracing identifies hemogenic endothelial cells in the adult mouse bone marrow

Jing-Xin Feng,[1] Mei-Ting Yang,[2, 3] Lili Li,[1] Caiyi C. Li[4], Ferenc Livák[4], Jack Chen[5], Yongmei Zhao[5], Dunrui Wang[1], Avinash Bhandoola[4], Naomi Taylor[6], and Giovanna Tosato[1,7,8*]

[1]Laboratory of Cellular Oncology, Center for Cancer Research, National Cancer Institute (NCI), National Institutes of Health, Bethesda, MD, 20892, USA

[2]School of Life Sciences, Northeast Normal University, Changchun, China

[3]Experimental Immunology Branch, Center for Cancer Research (CCR), National Cancer Institute (NCI), National Institutes of Health, Bethesda, MD, 20892, USA

[4]Laboratory of Genome Integrity, Center for Cancer Research, National Cancer Institute (NCI), National Institutes of Health, Bethesda, MD, 20892, USA

[5]Sequencing Facility Bioinformatics Group, Bioinformatics and Computational Science Directorate, Frederick National Laboratory for Cancer Research, Frederick, MD, 21702, USA

[6]Pediatric Oncology Branch, Center for Cancer Research (CCR), National Cancer Institute (NCI), National Institutes of Health, Bethesda, MD, 20892, USA.

[7]Senior author

[8]Lead contact

*Correspondence: tosatog@mail.nih.gov (G.T.) jing-xin.feng@nih.gov (J.F.)

SUMMARY

During mouse development, hematopoietic stem and progenitor cells (HSPC) originate from hemogenic endothelial cells (ECs) through a process of endothelial-to-hematopoietic transition. These HSPC are thought to fully sustain adult hematopoiesis. However, it remains unknown whether adult ECs retain hemogenic potential. Here we used in vivo genetic lineage tracking at population and single-cell (sc) levels, scRNA sequencing, and bone marrow transplantation to detect hemogenic ECs in adult mice. We identify and characterize a small population of bone marrow-resident, adult *Cdh5*/VE-Cadherin^{+} ECs that produce hematopoietic cell-progeny in vitro and in mice. These adult hemogenic ECs and their hematopoietic cell progeny can give rise to hematopoietic cells following adoptive transfer into adult mice. Furthermore, blood cells generated from adult and developmental ECs comparably home to peripheral tissues, where they similarly contribute to inflammatory responses. Thus, our results identify previously unrecognized bone marrow-derived adult hemogenic ECs that generate HSPC and functional mature blood cells.

KEYWORDS

Hematopoietic stem and progenitor cells, endothelial cells, hematopoiesis, endothelial to hemogenic transition, mesenchymal cells, blood, *Runx1*, *Col1a2*, single cell lineage tracing, single cell RNA sequencing

40 **INTRODUCTION**

41 During development, hemogenic ECs generate hematopoietic cells through a process of
42 endothelial-to-hematopoietic transition (EHT) at geographically defined anatomical sites[1-9]. At
43 these locations, the hemogenic ECs represent a small fraction of all ECs[10-12], and their
44 competency to produce hematopoietic stem and progenitor cells (HSPC) is temporally restricted
45 to short developmental windows, and the hemogenic potential differs[13-18]. In the dorsal aorta, the
46 hemogenic endothelium produces hematopoietic stem cells (HSC) and other multi-potent
47 progenitors between E10.5 and E11.5[17-19] that persist in the adult and are generally believed to
48 sustain adult hematopoiesis throughout life.

49 Efforts to reliably generate *ex vivo* HSC from Cdh5-expressing ECs identified difficulties
50 in reproducing the microenvironmental clues coming from the inductive niche cells[20-22] and have
51 generally relied on transcription factor-induced reprogramming of the ECs to drive
52 hematopoietic specification[23,24]. The transcription factor RUNX1, which marks the hemogenic
53 endothelium, can confer a hemogenic potential to embryonic ECs lacking such potential[25-28].
54 When transcription factors RUNX1, FOSB, GFI1, and SPI1 were co-expressed in adult murine
55 ECs co-cultured with "vascular niche ECs", EHT was induced in vitro producing HSC with
56 long-term self-renewal capacity[29]. A similar approach was used with human ECs enabling
57 hematopoietic specification[30].

58 An unresolved question is whether hemogenic ECs, thought to be mostly restricted to the
59 early stages of mouse development[12,23], may persist in the adult mouse[2,12,31,32]. Exploiting
60 advances in cell lineage tracking and single cell analyses[33,34], we report the identification of
61 hemogenic ECs in the adult mouse bone marrow (BM) that produce functional hematopoietic
62 progenitors and mature blood cells.

63 **RESULTS**

64 **Evidence that adult bone marrow ECs generate hematopoietic cells**

65 We assessed the hemogenic potential of ECs in adult mice using Cre-reporter-based lineage
66 tracing. Since *Cdh5*, encoding vascular endothelial cadherin (VE-Cadherin), is selectively
67 expressed by ECs, Cdh5-Cre^{ERT2} recombinase activity allows tracking the hematopoietic cell
68 output from adult hemogenic ECs[35,36]. Therefore, we generated three Cdh5-based lineage-tracing
69 models using inducible Cdh5-Cre^{ERT2}(PAC)[37,38] and Cdh5-Cre^{ERT2}(BAC)[39] mouse lines, in
70 combination with the Cre-reporter lines ZsGreen and mTmG (Figure S1A). We then treated
71 eight- to twelve-week-old mice with three doses of tamoxifen (10 mg·kg^{-1}, gavage) on
72 consecutive days, and four weeks later we evaluated peripheral blood and BM (Figure 1A).
73 Expectedly[36], most BM Endomucin^{+} ECs were ZsGreen^{+} in tamoxifen-treated Cdh5-
74 Cre^{ERT2}(PAC)/ZsGreen and Cdh5-Cre^{ERT2}(BAC)/ZsGreen mice, and virtually no ZsGreen^{+} ECs
75 were present in Cre negative or peanut oil-treated controls (Figures S1B and S1C). By flow
76 cytometry, >90% CD31^{+}VE-Cadherin^{+} BM ECs were tracked by tamoxifen-induced
77 fluorescence in the three mouse lines (Figure 1B; Figure S1D). A low-level tamoxifen-
78 independent reporter fluorescence was also detected in BM ECs, which was low in the mTmG
79 reporter line (Figure 1B), and higher in the ZsGreen reporter lines, previously attributed to
80 "basal" Cre^{ERT2} activity[40] (Figure S1D).

81 To evaluate the hemogenic potential of adult BM ECs, we analyzed the expression of the
82 hematopoietic marker CD45 in Cdh5-tracked cells. Notably, tracked CD45^{+} hematopoietic cells,
83 presumed progeny of VE-Cadherin^{+} ECs, were detected by flow cytometry in BM and blood of
84 mice from all three Cdh5-Cre^{ERT2} mouse lines (Figure 1C and D; Figures S1E and F;
85 representative flow cytometry gating in Figure S1G and H). Moreover, confocal microscopy

86 identified isolated ZsGreen^{+}CD45^{+} cells in BM (Figure S1I) and blood of tamoxifen-induced
87 mice (Figure 1E). Importantly, while a small fraction of fluorescent CD45^{+} cells were detected in
88 EGFP and ZsGreen (Figures 1C and D; and Figure S1D-F) reporter mice without tamoxifen, as
89 reported[40-43], the significant increase of tamoxifen-induced fluorescent CD45^{+} cells (Figure 1C
90 and 1D, Figure S1D-F) indicates the occurrence of Cdh5-Cre recombination in the adult mouse,
91 presumably tracking EHT. This tamoxifen-induced increase in CD45^{+}ZsGreen^{+} peripheral blood
92 mononuclear cells (PBMC) was also observed in individual mice (Figure S1J).

93 We tested the kinetics of tamoxifen-induced ZsGreen expression in BM ECs and PBMC
94 of Cdh5-Cre^{ERT2}(PAC)/ZsGreen mice (Figure 1F). By flow cytometry, virtually all BM ECs
95 were ZsGreen^{+} by day 4 after tamoxifen administration and this level persisted over 50 days.
96 Instead, the percentage of ZsGreen^{+} PBMCs increased more gradually, plateauing by day 14 and
97 this level persisted over 50 days of observation. This gradual increase is likely attributable to
98 tamoxifen-induced ZsGreen expression in hemogenic ECs.

99 Further analysis showed that most BM EGFP^{+}CD45^{+} cells in Cdh5-Cre^{ERT2}(PAC)/mTmG
100 mice were CD11b^{+}Ly6G^{+} granulocytes (48.85%) and CD11b^{+}Ly6G^{-} monocytes (32.06%), while
101 CD19^{+} B (2.46%) and CD3^{+} T (0.84%) lymphocytes were detected at lower frequencies (Figure
102 1G). All EGFP^{+} BM cell populations were significantly induced by tamoxifen administration,
103 including rare LSK (Lin^{-}Sca1^{+}cKit^{+}) progenitors (Figure 1H). Also, the peripheral blood of
104 tamoxifen-induced Cdh5-Cre^{ERT2}(PAC)/mTmG mice contained EGFP^{+} granulocytes and
105 monocytes, and fewer B and T lymphocytes (Figure S1K and L). Similarly, in ZsGreen-reporter
106 mice, tracked LSK progenitors, B lymphocytes, granulocytes, and monocytes were all present in
107 the BM and blood (Figure S2A-D).

108 We further characterized the tracked BM hematopoietic LSK stem/progenitors by flow
109 cytometry (Figure S2E). The results, displayed by Uniform Manifold Approximation and
110 Projection (UMAP) dimensional reduction, showed that the ZsGreen-tracked progenitor
111 population includes cell subsets defined phenotypically as hematopoietic stem and progenitor
112 cells (HSPC) (Figure 1I). Each ZsGreen^{+} progenitor population represented a similarly small
113 proportion of the corresponding non-tracked progenitor cell population (Figure 1J). These results
114 support the existence of EHT in the adult mouse contributing to generation of hematopoietic
115 progenitors and mature cells.
116
117 **Adult BM ECs cultured ex vivo generate transplantable HSPCs**
118 To investigate whether adult BM ECs can generate hematopoietic cells *ex vivo*, we cultured BM
119 cells isolated from tamoxifen-treated Cdh5-Cre/ZsGreen mice. Initially, BM single-cell (sc)
120 suspensions were cultured under two conditions (Figure 2A): (1) on "Primaria" pro-adhesive
121 flasks, and (2) on OP9 stromal cell[44] monolayers grown on gelatin-coated conventional tissue
122 culture flasks. To attempt recreating BM niches, fresh wild-type (WT) BM cells were added to
123 the ZsGreen-tracked BM cell cultures twice/week throughout the culture period (see Methods for
124 details). By week 8, BM cells cultured on "Primaria" dishes formed a confluent monolayer of
125 ZsGreen-tracked cells with a typical EC morphology, whereas BM cells cultured on OP9
126 monolayers exhibited a fibroblast-like morphology with the ZsGreen^{+} cells clustering in foci,
127 without forming a monolayer (Figure 2A). We visualized some ZsGreen-tracked (ZsGreen^{+})
128 cells in cultures of BM cells grown onto OP9 monolayers supplemented with fresh BM cells, but
129 not in cultures of BM cells grown onto "Primaria" surfaces supplemented with fresh BM cells

130 (Figure S2F). This hinted that the OP9 and BM cell culture system may allow hematopoietic
131 cells emergence from Cdh5-Cre/ZsGreen-tracked EC ex vivo.
132 To test this possibility, we generated a pool of BM cells (from 20 adult mice; age 10-18
133 weeks) and used the pool to derive 3 populations: sorted BM CD45^{-}VE-Cadherin^{+}ZsGreen^{+}
134 ECs; sorted CD45^{+}ZsGreen^{+} hematopoietic cells; and unsorted BM cell populations (Figure 2B).
135 We then cultured these 3 cell populations under the same conditions (OP9 monolater and
136 supplementation with fresh BM cells twice/week). After 8-week culture, flow cytometry analysis
137 detected CD45^{+}ZsGreen^{+} cells from the unsorted BM and the sorted CD45^{-}VE-
138 Cadherin^{+}ZsGreen^{+} cell cultures, but the CD45^{+}ZsGreen^{+} were virtually absent from the
139 CD45^{+}ZsGreen^{+} cell cultures (Figure 2C and 2D). These results show that CD45^{-}VE-
140 Cadherin^{+}ZsGreen^{+} ECs can generate CD45^{+}ZsGreen^{+} *ex vivo*. Notably, most (>80%)
141 CD45^{-}ZsGreen^{+} cells retained expression of VE-Cadherin and Endomucin, thereby confirming
142 their endothelial identity (Figure 2C, most right panel). Importantly, the virtual absence of
143 CD45^{+}ZsGreen^{+} cells in 8-week cultures of sorted CD45^{+}ZsGreen^{+} cells shows that pre-existing
144 CD45^{+}ZsGreen^{+} hematopoietic cells, derived from tamoxifen-dependent and independent
145 processes, are effectively removed during the extended culture. This further suggests that the
146 CD45^{+}ZsGreen^{+} hematopoietic cells detected in the CD45^{-}VE-Cadherin^{+}ZsGreen^{+} EC cultures
147 likely originated from ECs during the final week of culture.
148 Next, we tested whether the *ex vivo*-derived CD45^{+}ZsGreen^{+} cells are functional in
149 lethally irradiated recipients. To this end, we obtained unfractionated BM cells from 50
150 tamoxifen-treated Cdh5-Cre/ZsGreen mice, cultured the cells onto OP9 monolayers with fresh
151 BM supplementation, sorted the ZsGreen^{+} cells (96% of which were CD45^{+} by flow cytometry)
152 at the end of 8-week culture, and transplanted these cells into 8 lethally irradiated WT recipients;

153 5×10^3 cells; 2.5×10^3 cells; 1.25×10^3 cells; 6.25×10^2 cells, n=2/group (Figure 2E-G). Two mice
154 (recipients of 6.25×10^2 and 1.25×10^3 cells) died on days 4 and 6, but the remaining six mice
155 survived and remain well at the time of manuscript submission (12 weeks post-transplant). Ten
156 weeks post-transplant, peripheral blood WBC counts were within normal range in all surviving
157 transplant recipients, indicative of hematopoietic reconstitution (Figure 2H). Flow cytometry
158 revealed that 74.85% of PBMC were ZsGreen$^+$ (Figure 2I). Most myeloid cells (granulocytes
159 and monocytes, 91.97%) and B cells (93.78%) were ZsGreen$^+$, whereas only 30.63% of T cells
160 were ZsGreen$^+$, likely attributable to long-lived ZsGreen$^-$ T cells.
161 These results confirm that BM ECs propagated *ex vivo* onto OP9 monolayers with BM
162 cell supplementation produce hematopoietic cells and show that this output includes HSPC
163 capable of engrafting and generating hematopoietic cell progeny of myeloid and lymphoid
164 lineages in lethally irradiated recipients.
165
166 **Adult BM ECs can give rise to hematopoietic cells after transfer to conditioned recipients**
167 Next, we examined whether adult BM ECs are hemogenic in transplant recipients. To this end,
168 we FACS-sorted CD45$^-$VE-Cadherin$^+$ZsGreen$^+$ ECs from the BM of tamoxifen-pretreated (4
169 weeks prior to BM harvest) Cdh5-Cre^{ERT2}(PAC)/ZsGreen mice (Figure 3A; Figure S2G and
170 S2H) and transplanted these cells into adult WT C57Bl/6 mice untreated (PBS) or conditioned by
171 fluorouracil (5-FU treated) prior to transplant[45]. The choice of 5-FU conditioning rather than
172 lethal irradiation of adult mice was driven by previous experiments showing the difficulties at
173 reconstituting lethally myelo-ablated adult recipients with hemogenic yolk sac cells, which
174 reconstituted conditioned newborns[46]. Four weeks after transplant, we observed a significant
175 increase in the proportion of ZsGreen$^+$ ECs in the BM and ZsGreen$^+$CD45$^+$hematopoietic cells in

176 the BM and peripheral blood of the transplant recipients conditioned by 5-FU but not controls
177 (PBS) (Figure 3B and 3C; Figure S2I). These $CD45^+$ZsGreen-tracked cells in BM and blood
178 included granulocytes, monocytes, and lymphocytes (Figure 3D). Thus, BM-derived $CD45^-$VE-
179 $Cadherin^+ZsGreen^+$ cells, when transferred into 5-FU-conditioned recipients, gave rise to
180 detectable $CD45^+ZsGreen^+$ hematopoietic cells.

181 We further examined the effect of mouse age on the endothelial hemogenic potential by
182 treating the mice with tamoxifen between week 6 and 32 of age. Four weeks later (week 10 to 36
183 of age), we measured the percentage of ZsGreen-tracked $CD45^+$ hematopoietic cells in the BM.
184 We observed that tamoxifen inductions beyond week 10 of age resulted in a progressive decrease
185 of the $CD45^+$ hematopoietic cell output, and detected an inverse correlation (Pearson's r -0.63,
186 $P<0.0001$) between age and EC hemogenic potential (Figure 3E). This progressive decline of
187 $CD45^+$ cell output was not coupled with a loss of BM EC fluorescence, since virtually all BM
188 ECs were $ZsGreen^+$ throughout the duration of the experiment (Figure 3F), consistent with the
189 stability of Cre-mediated labeling of Cdh5-expressing cells [36]. These observations suggest an
190 age-related loss of hemogenic capability of BM ECs.

191 Additionally, we examined whether tracked hematopoietic cells from adult BM EC are
192 functional. Since lymphocyte trafficking from the peripheral blood to the peritoneal cavity is
193 critical for their function at this site[47,48], we first evaluated the spontaneous migration of tracked
194 $CD45^+$ hematopoietic cells to the peritoneal cavity. Compared to no-tamoxifen controls,
195 tamoxifen-treated Cdh5-Cre^{ERT2}(PAC)/ZsGreen mice displayed a significant increase of
196 $CD45^+ZsGreen^+$ monocytes, macrophages, and B1, B2, and T lymphocytes in the peritoneal
197 cavity (Figure S2J and S2K).

198 After inducing peritonitis with thioglycolate (TGL, 4 hours) in tamoxifen-treated Cdh5-
199 Cre^{ERT2}(PAC)/ZsGreen mice, the overall number of peritoneal leukocytes increased substantially
200 compared to untreated (PBS) controls (Figure 3G), mostly attributable to neutrophils (Figure
201 3H). In addition, the peritoneal ZsGreen^{+} and ZsGreen^{-} cell populations exhibited a similar cell
202 type distribution in TGL-treated mice (Figure 3I). We further examined *Escherichia coli* (K-12
203 strain) phagocytosis and reactive oxygen species (ROS) production in peritoneal cell exudates in
204 response to TGL (Figure 3J-3O). Both ZsGreen^{+} and ZsGreen^{-} peritoneal neutrophils and
205 macrophages comparably phagocytosed *Escherichia coli* and generated ROS (Figure 3J, 3K, 3M,
206 and 3N), except that the phagocytic and ROS production of ZsGreen^{+} macrophages was
207 somewhat higher than that of ZsGreen^{-} macrophages (Figure 3L and 3O).
208 Thus, Cdh5-tracked mature neutrophils and macrophages are functional at trafficking and
209 homing, and presumably capable of contributing to the host response to tissue inflammation.
210
211 **Adult EHT is independent of preexisting hematopoietic cell progenitors**
212 Faithful Cre-reporter lineage tracing requires that Cre recombinase activity be restricted to the
213 intended cell type[40]. In our system, Cdh5-Cre^{ERT2} is expected to drive recombination specifically
214 in ECs, as *Cdh5* is an established EC-specific marker. However, flow cytometry has occasionally
215 revealed rare VE-Cadherin^{+}CD45^{+} in mouse BM, exemplified in Figure S2G, potentially
216 reflecting double-positive cells. To address the possibility that cells co-expressing VE-
217 Cadherin/*Cdh5* and CD45/*Ptprc* exist in the mouse BM, we analyzed publicly available sc-
218 RNAseq data from adult mouse BM[49]. This analysis showed that only a small subset of
219 plasmacytoid dendritic cells (pDCs) co-express VE-Cadherin and CD45, but not HSPC or other
220 mature blood cells (Figure S3A-S3D). pDCs are terminally differentiated cells and unlikely

221 progenitors of tracked CD45^{+} multilineage progeny in our Cdh5-cre mice. Nonetheless, it is
222 plausible that other, currently unidentified, hematopoietic cells may also co-express *Cdh5*/VE-
223 Cadherin and *Ptprc*/CD45. We additionally considered the possibility that CD45^{+} progenitors
224 with functional Cre^{ERT2} activity may contaminate the sorted populations of Cdh5^{+}CD45^{-} BM
225 cells and could become fluorescent upon tamoxifen administration.

226 To address both possibilities, we performed transplant experiments with two populations
227 of Lin^{-}Sca1^{+}cKit^{+} (LSK) progenitors from tamoxifen untreated Cdh5-Cre^{ERT2}(PAC)/ZsGreen
228 mice: (1) a ZsGreen^{-} LSK population (>99% purity; Figure S3E-S3G) to assess whether
229 ZsGreen^{-} hematopoietic progenitors with a functional Cdh5-Cre^{ERT2} activity could become
230 fluorescent after tamoxifen, and (2) an LSK population enriched for ZsGreen^{+} cells (45.9%
231 purity, with the remaining 54.1% comprising ZsGreen^{-} LSK cells (Figure S3F)), to assess the
232 contribution of pre-tracked, tamoxifen-independent, hematopoietic progenitors. We then
233 transplanted these two LSK populations into lethally irradiated (11 Gy) WT C57Bl/6 recipients
234 (Figure 4A). Four weeks post-transplant, we administered tamoxifen and monitored the
235 peripheral blood for the presence of ZsGreen^{+} hematopoietic cells over six months.

236 Expectedly, all LSK recipients (ZsGreen^{-} LSKs or LSK enriched with ZsGreen^{+} cells)
237 showed successful hematopoietic reconstitution as evidenced by normal blood WBC counts by
238 10 weeks post-transplant (Figure 4B). Importantly, the mice transplanted with ZsGreen^{-} LSKs
239 did not produce ZsGreen^{+} PBMCs post-tamoxifen administration, indicating that the transplanted
240 LSKs and their progeny did not express tamoxifen inducible Cdh5-Cre^{ERT2} recombinase activity
241 (Figure 4C and 4D). Instead, the mice transplanted with ZsGreen^{+}-enriched LSKs displayed a
242 similar proportion of ZsGreen^{+} PBMCs prior to and after tamoxifen administration (Figure 4D),
243 indicating that the ZsGreen^{+} LSK has not expanded after tamoxifen administration. Collectively,

244 these results demonstrate that LSK progenitors in adult BM lack of tamoxifen-inducible Cdh5
245 expression and do not contribute to tamoxifen-induced adult EHT in our Cdh5-reporter mice.
246 Rather, these results strongly support the conclusion that Cdh5^{+}CD45^{-} ECs are a source of
247 hematopoietic cells in the adult mouse.

248 In additional experiments, we took advantage of the relative insensitivity of BM ECs
249 subsets to irradiation relative to BM hematopoietic cells[50] to examine the possibility that EC
250 surviving after lethal irradiation may be hemogenic. As a lethal dose of irradiation effectively
251 eliminates HSPCs and requires hematopoietic reconstitution for survival, we transplanted WT
252 (untracked) BM cells into lethally irradiated Cdh5-Cre/mTmG mice and treated the mice with
253 tamoxifen 4 weeks after transplantation (Figure 4E). Prior to tamoxifen administration, >99% of
254 PBMCs were not fluorescent, indicating that these cells derived from the transplanted WT BM
255 rather than host-derived (Figure 4F). After tamoxifen treatment, a progressive increase in EGFP^{+}
256 PBMCs was observed, reaching ~0.55% by six weeks, which included myeloid cells and B and T
257 lymphocytes (Figure 4F and 4G). Although we cannot exclude the possibility that rare EGFP^{+}
258 hematopoietic progenitor (tracked tamoxifen-dependently or independently) may have survived
259 the irradiation, the presence of EGFP^{+} hematopoietic cells in the circulation of lethally irradiated
260 Cdh5-Cre/mTmG mice suggests their derivation from radioresistant Cdh5^{+} ECs rather than from
261 radiosensitive hematopoietic progenitors. These results further support the view that adult ECs
262 possess hemogenic potential and can produce hematopoietic cells in vivo.
263

264 **Single cell tracking confirms the presence hemogenic ECs in adult BM**

265 To directly trace hematopoietic cell progeny arising from individual adult ECs, we exploited the
266 *PolyloxExpress* sc genetic barcoding system. We generated Cdh5-

267 Cre^{ERT2}/ZsGreen/*PolyloxExpress* mice, in which both the ZsGreen and Polylox transgenes are
268 inserted in the Rosa26 locus, such that individual ZsGreen^{+} cells contain a single Polylox
269 barcode[33,51,52]. To evaluate EC-derived hematopoietic cell output, we harvested BM from
270 tamoxifen-treated Cdh5-Cre^{ERT2}/ZsGreen/*PolyloxExpress* mice (n=3), sorted the ZsGreen^{+}VE-
271 Cadherin^{+}Endomucin^{+} (purity >99 %) and the ZsGreen^{+}VE-Cadherin^{-}Endomucin^{-}CD45^{+}
272 hematopoietic cells (purity >99%), mixed these populations (1:1 ratio; total 147,446 cells) and
273 processed for 10x Illumina Sequencing and PacBio sequencing (detailed in Methods). We
274 recovered sc transcriptome from 93,553 cells; of these, 4,072 cells had a barcode (Figure 5A,
275 Figure S5A, detailed in Methods).

276 Unsupervised clustering of sc transcriptome data revealed 34 clusters, 31 of which
277 remained after doublet removal (Figure 5B; Figure S5A-S5D). Cell clusters 0, 1, 22, and 13 were
278 annotated as "Endothelial cells" based on expression of the classical EC markers *Cdh5*, *Pecam1*,
279 *Kdr* and *Flt1*, and absence of *Ptprc*/CD45, *Runx1*, and the mesenchymal cell markers *Cxcl12*,
280 *Lepr*, *Pdgfrb*, and *Col1a2* expression (Figure 5B; Figure S4E). Cell cluster 14 was annotated as
281 "Mesenchymal type" based on co-expression of *Cxcl12*, *Lepr*, *Pdgfrb*, *Col1a2*, but expressed
282 *Runx1* and the EC markers *Cdh5* and *Pecam1* (Figure 5B; Figure S5E). The remaining cell
283 clusters included the hematopoietic progenitors and mature blood cells of various lineages
284 (Figure 5B; Figure S4E).

285 Barcode analysis revealed robust *Polylox* barcode diversity among cell populations,
286 including 296 "true" barcodes, defined as barcodes with low generation probability ($P_{gen} < 1\times10^{-}$
287 ^{4})[51] consistent with rare, unique recombination events (Figure S5A and S5B). Expectedly, "true"
288 barcodes linked HSPC to downstream progenitors and mature hematopoietic cells, validating the
289 system (Figure 5C).

290 Notably, 83 ECs (from “endothelial” cell clusters 0, 1, 22, and 13) were marked by “true”
291 barcodes, 31 of which linked EC to hematopoietic cells based on their shared barcode (Figure
292 5D). These hematopoietic cells linked to ECs by shared barcodes included HSPC, EPC, GMP,
293 and mature blood cells, encompassing granulocytes, monocytes, dendritic cells, B and T
294 lymphocytes, plasma cells, and pDCs (Figure 5D). These results provide direct evidence, at sc
295 resolution, that adult mouse BM ECs can generate hematopoietic progenitors and mature blood
296 cells.
297 Additionally, 30 “Mesenchymal type” cells (from cluster 14; co-expressing mesenchymal
298 cell markers, *Runx1*, and the EC markers *Cdh5* and *Pecam1*) were also marked by 13 “true”
299 barcodes, 9 of which were shared with hematopoietic cell progenitors (HSPC and Erythroid) and
300 mature blood cells (Figure 5E and F). Also, 6 “true” barcodes linked “Mesenchymal type” cells
301 to ECs (from clusters 0, 1, 22 and 13), suggesting either a shared precursor or derivation from
302 each other. Although it cannot be excluded that barcoding missed identification of mesenchymal
303 cell links to other ECs or cells, these results raise the possibility that certain BM “Mesenchymal
304 type” cells may produce hematopoietic cell progeny. Despite similarities of sc tracing results
305 linking ECs and “Mesenchymal type” cells to hematopoietic cells, these two cell populations
306 display a distinctive transcriptome profile (Figure 5G; Figure S4E).
307 Additional analysis of all tracked cells showed that several ECs and to a lower extent
308 “Mesenchymal type cells” shared “true” barcodes (Figure 5D-5F), indicating clonal expansion.
309 Transcriptome-based sc cell cycle analysis, confirmed the presence of ECs and “Mesenchymal
310 type cells” in the S and G2/M phases, albeit to a much lower degree than HSPC (Figure S5C).
311 Together, these results demonstrate at a sc level that adult BM ECs can generate hematopoietic
312 cell progeny of HSPC and mature blood cells. The results further raise the possibility that

313 “Mesenchymal type” cells, marked by a hybrid endothelial and stromal phenotype, may
314 represent an additional source of hemogenic activity in adult BM.
315
316 **Single cell transcriptome identifies a *Cdh5*$^{+}$*Col1a2*$^{+}$ *Runx1*$^{+}$cell population in the adult BM.**
317 To further characterize adult hemogenic cell populations, we analyzed publicly available
318 scRNAseq datasets comprising BM cells from adult mice (1-16 months of age)[53-59] and
319 embryonic caudal artery ECs (9.5–11.5 days post coitum)[24]. After quality control and
320 dimensional reduction, the remaining 434,810 cells clustered into 71 distinct populations (Figure
321 6A-D). Among the *Cdh5*-expressing endothelial clusters, two clusters, cluster 8 composed
322 predominantly of embryonic cells (98%) and cluster 50 composed largely of adult BM-derived
323 cells (95.5%) (Figure 6E), were notable in comprising cells co-expressing *Cdh5* and *Runx1*, a
324 transcription factor that marks the hemogenic EC identity during development[60] (Figure 6B).
325 We jointly analyzed the transcriptome from the publicly available embryonic cluster 8
326 and adult cluster 50 (Figure 6 A-C), and from our sc Polylox dataset, including adult clusters 14
327 (Mesenchymal-type) and adult EC clusters 0, 1, 13 and 22 (Figure 5B). All populations
328 expressed canonical EC markers (*Cdh5*, *Pecam1*, *Kdr*, *Flt1*), though at different levels, but
329 expression of *Runx1* was mostly confined to clusters 8, 50 and Polylox 14 (Figure 6F).
330 Interestingly, adult clusters 50 and Polylox 14 co-expressed the mesenchymal cell-associated
331 genes *Col1a2*, *Lepr*, *Cxcl12*, and *Pdgfrb*, distinguishing these two clusters from the embryonic
332 cluster 8 and adult Polylox clusters 0, 1, 13 and 22 (Figure 6F). Additionally, embryonic cluster
333 8 exhibited higher expression of key EHT-related transcription factors (FLI1, LMO2, TAL1,
334 ERG)[61-64], some of which were variably expressed by the Polylox clusters 0,1,13 and 22 (Figure
335 6F).

336 To explore whether cells expressing *Cdh5*, *Col1a2* and *Runx1* are unique to BM (Figure
337 6G), we looked at other adult mouse tissues. Analysis of public scRNAseq datasets from 11 adult
338 mouse tissues[65] showed that *Cdh5*, *Runx1*, and *Col1a2* expressing ECs are largely restricted to
339 the BM, with only 3 such cells detected out of ~32,000 EC from other tissues (Figure 6H and
340 I)[65]. These observations, together with the Polylox sc tracing experiments, indicate that adult
341 mouse BM harbors a cell population with mixed endothelial and mesenchymal phenotype
342 marked by *Runx1*, *Col1a2* and *Cdh5* expression and raises the possibility that this population has
343 hemogenic potential.
344
345 ***Col1a2* and *Runx1* expression in BM ECs**
346 To evaluate a potential contribution of *Col1a2* expression to EHT in adult BM, we generated the
347 mouse lines Col1a2-Cre^{ERT2}/mTmG and Col1a2-Cre^{ERT2}/ZsGreen to track cells expressing the
348 *Col1a2* gene (Figure S6A). Four weeks after tamoxifen administration, the BM of Col1a2-
349 Cre^{ERT2}/ZsGreen mice contained abundant ZsGreen^{+} cells (Figure S6B). By flow cytometry, a
350 subset of these BM Col1a2-tracked ZsGreen^{+} cells were VE-Cadherin^{+}CD45^{-} and RUNX1^{+}
351 consistent with an endothelial identity and perhaps hemogenic potential (Figure S6C).
352 Noteworthy, a similar subset of VE-Cadherin^{+}CD45^{-}RUNX1^{+} cells was detected in BM of adult
353 WT C57Bl/6 mice (Figure S6D) and in BM of Cdh5-Cre^{ERT2}(PAC)/ZsGreen mice after
354 tamoxifen treatment (Figure S6E).
355 To evaluate hemogenic potential, we looked for Col1a2-tracked CD45^{+} hematopoietic
356 cells in Col1a2-Cre^{ERT2}/mTmG and Col1a2-Cre^{ERT2}/ZsGreen mouse lines after tamoxifen
357 treatment. In both these mouse lines, we detected CD45^{+} hematopoietic cells tracked by EGFP or
358 ZsGreen fluorescence in BM and blood, which were rare but significantly more abundant than in

359 control mice not treated with tamoxifen (Figure 7A and B; Figure S6F-H). These results
360 indicated that a proportion of the Col1a2-tracked cells in the adult mouse are hemogenic.
361 To further evaluate this possibility, we first sorted VE-Cadherin^{+}CD45^{-} ZsGreen
362 (Col1a2)$^{+}$ cells from the BM of tamoxifen-induced adult Col1a2-Cre^{ERT2}/ZsGreen mice (Figure
363 S7A), examined expression of selected genes, and used these cells in transplant experiments. The
364 sorted VE-Cadherin^{+}CD45^{-} ZsGreen (Col1a2)$^{+}$ cells expressed *Cdh5*, *Col1a2*, *Cxcl12*, and *Runx1*
365 mRNAs distinctively from other BM cell population (Figure S7B), but resembled the BM
366 hemogenic population annotated as "mesenchymal-type" (cluster 14) identified by Polylox s.c
367 sequencing (Figure 5G; Figure S4E) and subsets of adult BM Cdh5^{+} cells identified in public
368 adult datasets (Figure 6E and F).
369 We transplanted the BM VE-Cadherin^{+}CD45^{-} ZsGreen (Col1a2)$^{+}$ cells (1×10^{4}
370 cells/mouse) into 5-FU-conditioned adult WT C57Bl/6 recipients and looked for tracked CD45^{+}
371 cells in the BM and blood (Figure 7C). Four weeks after transplantation, BM and peripheral
372 blood of transplant recipients contained ZsGreen^{+}CD45^{+} cells (Figure 7D; Figure S7C and D),
373 indicating that the transplanted ZsGreen^{+} (Col1a2)-tracked CD45^{-} ECs had produced CD45^{+}
374 hematopoietic cell progeny. These ZsGreen^{+}CD45^{+} cells in the recipient mice comprised mainly
375 granulocytes and monocytes, and few B and T lymphocytes (Figure 7E). These results indicate
376 that Col1a2-tracked ECs, like Cdh5(VE-Cadherin)-tracked ECs, can give rise to hematopoietic
377 progeny in vivo, but display a more restricted multilineage potential compared to ECs from
378 Cdh5-Cre^{ERT2}(PAC)/ZsGreen mice.
379 In additional experiments, we evaluated the role of *Runx1* expression in adult BM
380 hemogenic EC since our analyses identified *Runx1* as a putative marker of adult EHT (Figure 6E
381 and F; Figure S4E). Therefore, we generated a Runx1$^{EC\text{-}KI}$ mouse line (*Cdh5*-

382 *Cre^{ERT2}/ZsGreen/Runx1-Knock-In*), in which Cre-mediated excision of a floxed STOP codon
383 enables co-expression of ZsGreen and *Runx1* in ECs upon tamoxifen induction (Figure S7E)[66].
384 In these Runx1^{EC-KI} mice, tamoxifen treatment increased significantly the frequency of ZsGreen^{+}
385 cells in PBMC over 60 weeks compared to control tamoxifen-treated (Cdh5-Cre^{ERT2}/ZsGreen)
386 mice (Figure 7F).

387 Since these circulating ZsGreen-tracked cells presumably represent hematopoietic cell
388 progeny of ECs co-expressing ZsGreen and *Runx1*, we tested the hemogenic potential of these
389 tamoxifen-induced BM EC ex vivo. Using the culture system that successfully supported ex vivo
390 hematopoiesis in Cdh5-tracked BM (Figure 2A-H), we now compared the hemogenic potential
391 of BM cells from tamoxifen pretreated Runx1^{EC-KI} mice to that of BM cells from tamoxifen
392 pretreated Cdh5-Cre^{ERT2}/ZsGreen) mice. We detected a significantly greater number of ZsGreen^{+}
393 clusters in cultures from Runx1^{EC-KI} BM cells compared to control BM cells (Figure 7G and H),
394 and flow cytometry showed that more CD45^{+}ZsGreen^{+} hematopoietic cells were produced in
395 cultures of Runx1^{EC-KI} BM cells compared to BM from controls (Figure 7I and J). Although we
396 cannot exclude the possibility that RUNX1 promotes EC proliferation in culture, these results
397 support a role of RUNX1 in promoting adult EHT.

398 **DISCUSSION**

399 Our results provide evidence for the presence of ECs with hemogenic potential in the adult
400 mouse BM. Previously, hemogenic ECs were detected during embryonic development or
401 perinatally but not thereafter[1-9,67]. The current findings argue that EHT is not limited to the
402 prenatal or perinatal development but is present up to 28 weeks after birth, decreasing thereafter.
403 This conclusion is supported by Cdh5-based bulk and Polylox sc lineage tracking, culture of

404 hemogenic ECs, transplant analyses and characterization of EC-derived hematopoietic cell
405 progeny, which link key features of adult EHT to embryonic EHT[25-28,68].
406 Previous experiments found that EHT, present in the late fetus/neonatal BM, disappears
407 shortly after birth[67]. This contrasts with the current experiments showing persistence of adult
408 EHT well beyond 20 weeks of age. The divergent results likely stem from functional differences
409 of the Cdh5-based tracking systems. In the previous experiments, attempts to activate Cdh5-
410 fluorescence in BM ECs by injecting tamoxifen at different time-points after birth were
411 unsuccessful starting 20 days after birth. Expectedly, the absence of tamoxifen-induced
412 fluorescence in BM ECs was associated with the absence of traced hematopoietic cell output
413 from these cells. In the current experiments and those of others[36], tamoxifen administration after
414 10, 20, and 30 weeks of age consistently induces fluorescence in most BM ECs. We conclude
415 that the absence of adult EHT had not been firmly established.
416 Adult hemogenic ECs identified here express *Cdh5*, *Pecam1*, *Kdr*, and *Flt1*, resembling
417 other BM EC populations and embryonic hemogenic ECs[69]. However, the current studies
418 identify yet another, small hemogenic cell population in the adult BM, distinctive in co-
419 expressing typical EC markers, *Cdh5* and *Pecam1*, and the mesenchymal-type markers *Lepr*,
420 *Col1a2* and *Cxcl12*. These two hemogenic populations are clonally linked, but it is currently
421 unclear whether they have a common progenitor, or one population derives from the other.
422 ECs derive from two sources during development: the splanchnic mesoderm that gives
423 rise to the primitive aorta where ECs located on the aortic floor are hemogenic[68], and the somites
424 from the paraxial mesoderm, that produce ECs contributing the endothelial vascular network of
425 the trunk and limb[70,71]. Somite-derived ECs are not hemogenic in situ, but they can transiently
426 acquire a hemogenic potential when variously induced[72] and may also include a cell subset with

427 hemogenic potential[73]. They can also express *Runx1* and trigger aortic hematopoiesis from
428 hemogenic ECs in zebrafish[74] and in the chick[68]. Besides generating hemogenic ECs, blood and
429 other tissues, the mesoderm in conjunction with the neural crest, gives rise to mesenchymal stem
430 cells (MSCs) and perhaps a precursor of both MSCs and ECs[75-77]. However, MSCs do not
431 produce blood cells, although they can differentiate into many other tissues[78], and their potential
432 for endothelial differentiation remains controversial[79-82]. By contrast, endothelial to
433 mesenchymal transition (EndMT) is a well-established process in development and disease
434 states[83].

435 It was suggested that the transient wave of EHT occurring in the BM of the late fetus and
436 perinatally may serve to mitigate the slow HSC colonization of BM from the fetal liver or
437 perhaps prepare the BM niches to accommodate the incoming HSC from the liver, but a function
438 has not yet been firmly established[67]. Similarly, the function of adult BM EHT identified here is
439 currently unclear. We hypothesize that adult EHT plays a role under conditions of hematopoietic
440 stress or disease rather than under steady-state conditions, but this will need future investigation.
441 Interestingly, previous studies found that subsets of EC can regenerate after irradiation that has
442 eliminated HSC[45], and we traced the emergence of some hematopoietic cells from ECs that
443 persisted after lethal mouse irradiation. We also found that 5-FU treatment was required for the
444 successful engraftment and function of adult hemogenic ECs suggesting that this population may
445 require inductive signals from a BM that is recovering from an insult[45,84]. The identification of
446 such inductive factors may enable effective propagation of BM hemogenic ECs ex vivo and
447 motivate a search for hemogenic ECs in human BM.

448 Altogether, our results provide evidence for a previously unrecognized capacity of ECs in
449 the adult mouse BM to generate blood cells. These results suggest that hematopoiesis in the adult

450 mouse may arise through the contribution of cells and processes beyond the HSCs generated
451 through aortic EHT during development and BM EHT perinatally.
452
453 **Limitations of the study**
454 A limitation of our study is that the function of adult EHT is currently unknown. Under steady-
455 state conditions, the hematopoietic cell output from adult EHT is low in comparison to that of
456 embryonic EHT, which effectively sustains adult hematopoiesis, and our experiments detected
457 no functional differences between hematopoietic cells from embryonic and adult EHT. To
458 address this limitation, we will examine whether adult EHT is a greater contributor to adult
459 hematopoiesis when stress is imposed on the adult hematopoietic system, and more fully
460 characterize the cell populations arising from adult EHT, focusing on minor cell population
461 known to serve critical functions in specific settings. Another limitation of our study is that we
462 could not extend the in vivo single-cell PolyloxExpress genetic lineage tracing to the ex vivo
463 single-cell genetic lineage tracing due to technical limitations of the PolyloxExpress system.
464 Finally, rigorous serial transplantation experiments, including CD45.1/CD45.2 competitive
465 repopulation assays, will be necessary to conclusively determine whether bona fide long-term
466 hematopoietic stem cells are generated by adult hemogenic endothelial cells both *in vivo* and *ex*
467 *vivo*.

468 **RESOURCE AVAILABILITY**

469 **Lead contact**
470 Further information and requests for resources and reagents should be directed to and will be
471 fulfilled by the lead contact, Giovanna Tosato (tosatog@mail.nih.gov).
472

473 **Materials availability**

474 This study did not generate new unique reagents.

475

476 **Data and code availability**

477 The results of scRNAseq and PacBio SmrtSeq of Polylox barcodes are deposited in NCBI SRA
478 (PRJNA1079369, public at time of publication). A custom script was used to retrieve cell
479 indexes from the PolyloxExpress amplicons (https://github.com/CCRSF-IFX/SF_Polylox-BC).
480 Bash, R, and Python codes are available from the corresponding author upon reasonable request.

481

482 **ACKNOWLEDGEMENTS**

483 This project is supported by the Intramural Program of CCR, NCI, NIH. The findings are those
484 of the authors and do not necessarily represent the official views of the NIH or the Department of
485 Health and Human Services. This work used the computational resources of the NIH High
486 Performance Computing (HPC) Biowulf cluster (*http://hpc.nih.gov*) and Frederick Research
487 Computing Environment (FRCE). Flow cytometry and cell sorting were performed at the CCR
488 Flow Cytometry Core Facility; microscopy analyses at the CCR Microscopy Core Facility in
489 Building 37 of the NCI, NIH. We thank Drs. Ralf Adams and Manfred Boehm for mouse line
490 *Cdh5-Cre^{ERT2}(PAC)*; Drs. Yoshiaki Kubota and Yosuke Mukoyama for mouse line *Cdh5-*
491 *Cre^{ERT2}(BAC)*; Dr. Hans-Reimer Rodewald for the *PolyloxExpress* mouse line. We thank Dr. S.
492 Banerjee, Dr. S. Siddiqui and Ms. K. M. Wolcott for flow cytometry support; Dr. M. Kruhlak
493 and Mr. L. Lim for confocal microscopy support and Mr. A. Abdelmaksoud for bioinformatics
494 assistance. We thank Drs. D. Lowy, R. Yarchoan, M. DiPrima and H. Ohnuki for thoughtfully
495 commenting on aspects of this work.

496

497 ## AUTHOR CONTRIBUTIONS

498 Concept and design: J-X.F. and G.T. Acquisition, analysis, or interpretation of data: J-X.F., G.T.,
499 C.L., F.L., N.T., A.B., L.L, M-T.Y., D.W., J.C., and Y.Z. G. Drafting of the manuscript: J-X.F.,
500 G.T. Critical revision of the manuscript for important intellectual content: J-X.F., G.T., A.B. and
501 N.T.

502

503 ## DECLARATION OF INTERESTS

504 The authors declare no competing financial interests.

505

506 ## SUPPLEMENTAL INFORMATION

507 Document S1. Figures S1–S7

508 ## FIGURE TITLES AND LEGENDS

509 **Figure 1. Lineage tracking discloses a contribution of endothelial cells to hematopoiesis in**
510 **adult BM**

511 (A) Experimental design: tamoxifen was administered to 8- to12-week-old Cdh5-Cre mice to
512 induce fluorescent labeling of VE-Cadherin^{+} cells and their cell progeny. Four weeks later, BM
513 and blood were analyzed.

514 (B) CD31^{+}EGFP^{+} BM ECs in Cre^{-} mice (n=10) and Cre^{+} mice treated with oil (n=13) or
515 tamoxifen (n=10); flow cytometry results.

516 (C and D) $CD45^+EGFP^+$ cells in BM and blood from Cre^- mice (n=8) and Cre^+ mice treated with
517 oil (n=6-10) or tamoxifen (n=15-18). Representative flow cytometry gating in Figure S1G.
518 (E) Representative blood smear from a tamoxifen-treated Cdh5-Cre^{ERT2}(PAC)/ZsGreen mouse
519 showing $ZsGreen^+CD45^+DAPI^+$ cells (arrows).
520 (F) Kinetics of $ZsGreen^+$ cell detection in BM ECs ($CD45^-$VE-$Cadherin^+$) and blood white blood
521 cells (WBC) post-tamoxifen; mouse n=8-10/group).
522 (G) $EGFP^+$ B and T-lymphocytes, granulocytes, and monocytes in BM of tamoxifen-treated mice
523 (n=14) as percent of total $EGFP^+$ cells; 3 experiments.
524 (H) $EGFP^+$ BM LSK, lymphocytes, granulocytes, and monocytes as percent of total $EGFP^{+/-}$ cell
525 type; Cdh5-Cre^{ERT2}(PAC)/mTmG mice (oil n=10; tamoxifen n=15), 3 experiments.
526 (I) UMAP plots of Lin^- BM HSPC from tamoxifen-treated Cdh5-Cre^{ERT2}(PAC)/ZsGreen mice
527 (n=26; 1 femur/mouse) showing FlowSOM clustering of all ($ZsGreen^{+/-}$) and $ZsGreen^+$
528 populations.
529 (J) Violin plots showing $ZsGreen^+$ cell distribution across HSPC subsets from (I).

530 Dots represent individual mice; data shown as mean±SD except shown as median in (G). *$p <$
531 0.05, **$p < 0.01$, ***$p < 0.001$ by Student's *t* test.

532

533 **Figure 2. BM ECs generate engraftable hematopoietic cells ex vivo**
534 (A) BM cells from tamoxifen-treated mice were cultured on high-attachment Primaria flasks or
535 OP9 cell monolayers. Representative images show $ZsGreen^+$ cells at weeks 1, 3, and 8.
536 (B) Workflow for culturing unsorted and sorted BM cell populations. All cells were cultured (8
537 weeks) on OP9 cell monolayers supplemented with WT BM cells. Culture medium and floating
538 cells were removed twice/week for 7 weeks. At the start of week 8, one final WT BM and

539 medium supplementation was implemented prior to harvest at the end of week 8. Representative
540 image (bottom left) shows sorted ZsGreen$^+$ ECs on OP9 monolayer after 4 weeks of culture.
541 (C and D) Representative flow cytometry plots (C) and quantification (D) of CD45$^+$ZsGreen$^+$
542 cells from each of the 8-week cultures (n=5).
543 (E) Floating/loosely adherent ZsGreen$^+$ cells from unsorted BM 8-week cell cultures were sorted
544 and transplanted (5×10^4, 2.5×10^4,1.25×10^4 or 6.25×10^3 cells) into lethally irradiated (11 Gy) WT
545 mice (n=2/group).
546 (F - G) Representative image (F) and quantification (G) of low-adherent cells harvested after 8
547 weeks of culture, showing that >95% of ZsGreen$^+$ low-adherent cells are CD45$^+$.
548 (H and I) WBC counts (F) and percent ZsGreen$^+$ and ZsGreen$^-$ cells (G) in blood of transplant
549 recipients 10 weeks post-transplant (n=6); WT controls (no irradiation or transplant; n=5).
550 Dots represent individual mice. Data are shown as mean ± SD. ns, not significant by Student's *t*
551 test.
552
553 **Figure 3. Adult BM endothelial cells give rise to hematopoietic cells following transfer into**
554 **conditioned recipients**
555 (A) Transplant experiment: donor ECs from BM of tamoxifen-treated mice were FACS-sorted
556 and transplanted into WT C57Bl/6 recipients conditioned with 5-FU or PBS.
557 (B) ZsGreen$^+$ ECs detected in BM of 5-FU-conditioned (n=5) or PBS-conditioned (n=15)
558 recipients of ECs 4 weeks post-transplant.
559 (C and D) ZsGreen$^+$CD45$^+$ cells (C) and cell type distribution (D) in the BM and blood of 5-FU-
560 conditioned transplant recipients of BM ECs or no cell controls (n=5/group).

561 (E and F) Age-dependent decline of ZsGreen^{+}CD45^{+} cells (E) but not ZsGreen^{+}VE-Cadhenin^{+}

562 cells (F) in the BM of Cdh5-Cre^{ERT2}(BAC)/ZsGreen mice (n=35) treated with tamoxifen 4-weeks

563 prior to harvest.

564 (G and H) Cell number (G; mouse n=8-12) and cell type distribution (H; mouse n=6) in the

565 peritoneal cavity (PerC) of PBS- or thioglycolate (TGL)-pretreated (4 hours) mice.

566 (I) ZsGreen^{+} and ZsGreen^{-} PerC cell types in TGL-pretreated mice (n=12).

567 (J) Representative histograms depicting pHrodo Red fluorescence detection of E-Coli

568 phagocytosis.

569 (K and L) E. coli^{+} phagocytosis by ZsGreen^{+} and ZsGreen^{-} PerC neutrophils (K) and

570 macrophages (L) in TGL-pretreated mice (n=4).

571 (M) Representative histograms depicting CellRox Orange fluorescence for cell-associated ROS

572 detection.

573 (N and O) CellRox mean fluorescence intensity (MFI) in ZsGreen^{+} and ZsGreen^{-} PerC

574 neutrophils (N) and macrophages (O) in TGL-pretreated mice (n=4).

575 Dots represent individual mice. Data are shown as mean ± SD. *$p < 0.05$, ***$p < 0.001$, ns, not

576 significant by Student's *t* test.

577

578 **Figure 4. Independence of adult EHT from preexisting HSPC**

579 (A) Transplantation experiment: donor LSK sorting, recipient irradiation, transplantation,

580 tamoxifen treatment, and analysis.

581 (B-D) Blood WBC counts (B), percent ZsGreen^{+} PBMC (C), and time course of ZsGreen^{+}

582 PBMC detection (D) in transplant recipients of ZsGreen^{-} LSK (5×10^{4} or 2.5×10^{4} cells/mouse;

583 n=3/group) and ZsGreen-enriched LSKs (2.8×10^3 cells/mouse; n=2). Results in B and C are from
584 week 24 post-tamoxifen.
585 (E) Experiment: WT BM transplantation (BMTP) into lethally irradiated Cdh5-Cre/mTmG mice
586 (n=9). Four weeks later, tamoxifen was administered; blood was monitored for 16 weeks.
587 (F and G) $EGFP^+$ PBMC detection before and after tamoxifen or peanut oil administration (F)
588 and cell type distribution of $EGFP^+$ and $EGFP^-$ PBMCs at week 12 post-tamoxifen or peanut oil
589 (G) in Cdh5-Cre/mTmG recipients (n=9) of WT BM (5×10^6 cells).
590 Dots represent individual mice. Data are shown as mean ± SD.
591
592 **Figure 5. Polylox sc lineage tracing links adult BM ECs to hematopoietic progenitors and**
593 **mature blood cell progeny**
594 (A) Schematic of Polylox barcode and transcriptome profiling. FACS-enriched ECs
595 ($ZsGreen^+$VE-$Cadherin^+$$Endomucin^+$) and EC-depleted ($ZsGreen^-$VE-$Cadherin^-$$Endomucin^-$) BM
596 cells from tamoxifen-treated Cdh5-CreERT2/ZsGreen/PolyloxExpress mice (n=3, 10 week-old
597 at the time of tamoxifen treatment) were mixed (1:1), and encapsulated (147,446 cells loaded;
598 93,553 processed). Indexed cDNA was used for scRNA-seq and barcode detection by PacBio
599 sequencing after nested PCR enrichment; barcode-transcriptome integration was accomplished
600 via shared cell indices.
601 (B) UMAP clustering and cell type annotation. Clusters 0, 1, 13, and 22 comprise ECs; cluster 14
602 comprises Mesenchymal-type cells.
603 (C – E) Heatmaps showing "true" Polylox barcodes (pGen < 1×10^{-4}) linking HSPCs to
604 hematopoietic cells (C), ECs to hematopoietic and other cells (D), and Mesenchymal-type cells
605 to other cells (E). The numbers within the colored boxes identify cell number; the labels at the

606 bottom of each column denote the barcode shared by all cells in that column; the number on the
607 right side the heatmaps reflects the total number of cells in each row.
608 (F) UpSet plot showing cells (identified by colored dots) sharing the same "true" barcode
609 (identified by lines connecting the colored dots); bar graph at the top of the plot reflects (height
610 and number on each bar) the number of "true" barcodes. Colors of dots: EC (red), Mesenchymal-
611 type (orange), ECs connecting with Mesenchymal-type cells (blue), cells other than ECs and
612 Mesenchymal-type cells (black).
613 (G) Violin plots showing selected gene expression profile in Mesenchymal-type cells (cluster 14)
614 and ECs (clusters 0, 1, 13, 22 combined).
615
616 **Figure 6. Sc transcriptomic analysis of prospective hemogenic ECs**
617 (A) UMAP clustering of 434,810 cells from eight public scRNA-seq datasets.
618 (B) Dot plot showing relative Cdh5 and Runx1 co-expression across clusters; clusters 8 and 50
619 co-express both genes.
620 (C) UMAP highlighting clusters 8 and 50; all other clusters shown in grey.
621 (D) Violin plots of doublet scores across Leiden clusters. Clusters 50 and 8 show no evidence of
622 doublet enrichment.
623 (E) Datasets proportional contribution to clusters 50 and 8; each dataset is color-coded.
624 (F) Dot plot showing expression of selected marker genes in clusters 50 and 8 (from the public sc
625 RNA-seq datasets listed in Figure 7D) and from clusters 0, 1, 13, 22 and 14 (from Polylox
626 scRNA-seq; Figure 5B). Results reflect mean expression and fraction of cells in group.
627 (G) Cdh5, Runx1 and Col1a2 co-expression in the indicated clusters as a fraction of cells in the
628 cluster.

629 (H and I) t-SNE plot of ECs from 11 murine tissues (G) and Venn diagram (H) showing rare co-
630 expression of Cdh5, Runx1, and Col1a2 in these tissues.
631
632 **Figure 7. Contribution of *Col1a2* and *Runx1* expression to ECs hemogenic activity**
633 (A and B) Percent $EGFP^{+}CD45^{+}$ cells in BM and blood of tamoxifen-treated (n=6) or oil-treated
634 (n=5) Col1a2-Cre^{ERT2}/mTmG mice (A) and tamoxifen-treated (n=4) or oil-treated (n=3) Col1a2-
635 Cre^{ERT2}/ZsGreen mice (B). Cre-control mice (n=5 in A, and n=2 in B).
636 (C) Transplant experiment: sorted VE-$Cadherin^{+}CD45^{-}ZsGreen^{+}/Col1a2^{+}$ cells from tamoxifen-
637 treated Col1a2-Cre^{ERT2}/ZsGreen mice are transplanted into 5-FU-conditioned WT recipients.
638 (D and E) Detection (D) and characterization (E) of $ZsGreen^{+}CD45^{+}$ cells in BM and blood of
639 WT 5-FU-conditioned mice (n=5), 4 weeks post-transplant of VE-
640 $Cadherin^{+}CD45^{-}ZsGreen^{+}/Col1a2^{+}$ cells. Control FU-conditioned WT mice (n=4) received no
641 cell transplant (D).
642 (F) Time course of $ZsGreen^{+}$ PBMC detection in control (Cdh5-Cre^{+}/$ZsGreen^{+}$) and $Runx1^{EC\text{-}KI}$
643 (Cdh5-Cre^{+}/$ZsGreen^{+}$/Runx1-KI) mice (n=10 per group).
644 (G and H) Representative images (G) and quantification (H) of $ZsGreen^{+}$ cells from OP9 cell-
645 supported cultures of BM cells from tamoxifen-treated Cdh5-Cre^{+}/$ZsGreen^{+}$ (n=11) and
646 $Runx1^{EC\text{-}KI}$ mice (n=5).
647 (I and J) Representative flow cytometry plots (I) and quantification (J) of $CD45^{+}ZsGreen^{+}$ cells
648 from OP9 cell-supported BM cell cultures (n=5/group).
649 Dots represent individual mice. Data are shown as mean ± SD. **$p<0.01$, ***$p < 0.001$ by
650 Student's t test.
651

652 **REFERENCES**

653 1. Jaffredo, T., Gautier, R., Eichmann, A., and Dieterlen-Lievre, F. (1998). Intraaortic
654 hemopoietic cells are derived from endothelial cells during ontogeny. Development *125*,
655 4575-4583. 10.1242/dev.125.22.4575.

656 2. Zovein, A.C., Hofmann, J.J., Lynch, M., French, W.J., Turlo, K.A., Yang, Y., Becker,
657 M.S., Zanetta, L., Dejana, E., Gasson, J.C., et al. (2008). Fate tracing reveals the
658 endothelial origin of hematopoietic stem cells. Cell Stem Cell *3*, 625-636.
659 10.1016/j.stem.2008.09.018.

660 3. Bertrand, J.Y., Chi, N.C., Santoso, B., Teng, S., Stainier, D.Y., and Traver, D. (2010).
661 Haematopoietic stem cells derive directly from aortic endothelium during development.
662 Nature *464*, 108-111. 10.1038/nature08738.

663 4. Boisset, J.C., van Cappellen, W., Andrieu-Soler, C., Galjart, N., Dzierzak, E., and Robin,
664 C. (2010). In vivo imaging of haematopoietic cells emerging from the mouse aortic
665 endothelium. Nature *464*, 116-120. 10.1038/nature08764.

666 5. Yokomizo, T., and Dzierzak, E. (2010). Three-dimensional cartography of hematopoietic
667 clusters in the vasculature of whole mouse embryos. Development *137*, 3651-3661.
668 10.1242/dev.051094.

669 6. Chen, M.J., Li, Y., De Obaldia, M.E., Yang, Q., Yzaguirre, A.D., Yamada-Inagawa, T.,
670 Vink, C.S., Bhandoola, A., Dzierzak, E., and Speck, N.A. (2011). Erythroid/myeloid
671 progenitors and hematopoietic stem cells originate from distinct populations of
672 endothelial cells. Cell Stem Cell *9*, 541-552. 10.1016/j.stem.2011.10.003.

673 7. Frame, J.M., Fegan, K.H., Conway, S.J., McGrath, K.E., and Palis, J. (2016). Definitive
674 Hematopoiesis in the Yolk Sac Emerges from Wnt-Responsive Hemogenic Endothelium

675 Independently of Circulation and Arterial Identity. Stem Cells *34*, 431-444.
676 10.1002/stem.2213.
677 8. Rhodes, K.E., Gekas, C., Wang, Y., Lux, C.T., Francis, C.S., Chan, D.N., Conway, S.,
678 Orkin, S.H., Yoder, M.C., and Mikkola, H.K. (2008). The emergence of hematopoietic
679 stem cells is initiated in the placental vasculature in the absence of circulation. Cell Stem
680 Cell *2*, 252-263. 10.1016/j.stem.2008.01.001.
681 9. Nakano, H., Liu, X., Arshi, A., Nakashima, Y., van Handel, B., Sasidharan, R., Harmon,
682 A.W., Shin, J.H., Schwartz, R.J., Conway, S.J., et al. (2013). Haemogenic endocardium
683 contributes to transient definitive haematopoiesis. Nat Commun *4*, 1564.
684 10.1038/ncomms2569.
685 10. Goldie, L.C., Lucitti, J.L., Dickinson, M.E., and Hirschi, K.K. (2008). Cell signaling
686 directing the formation and function of hemogenic endothelium during murine
687 embryogenesis. Blood *112*, 3194-3204. 10.1182/blood-2008-02-139055.
688 11. Marcelo, K.L., Goldie, L.C., and Hirschi, K.K. (2013). Regulation of endothelial cell
689 differentiation and specification. Circ Res *112*, 1272-1287.
690 10.1161/CIRCRESAHA.113.300506.
691 12. Hirschi, K.K. (2012). Hemogenic endothelium during development and beyond. Blood
692 *119*, 4823-4827. 10.1182/blood-2011-12-353466.
693 13. Yoshimoto, M., Porayette, P., Glosson, N.L., Conway, S.J., Carlesso, N., Cardoso, A.A.,
694 Kaplan, M.H., and Yoder, M.C. (2012). Autonomous murine T-cell progenitor
695 production in the extra-embryonic yolk sac before HSC emergence. Blood *119*, 5706-
696 5714. 10.1182/blood-2011-12-397489.

697 14. Lin, Y., Yoder, M.C., and Yoshimoto, M. (2014). Lymphoid progenitor emergence in the
698 murine embryo and yolk sac precedes stem cell detection. Stem Cells Dev *23*, 1168-1177.
699 10.1089/scd.2013.0536.
700 15. Iturri, L., Freyer, L., Biton, A., Dardenne, P., Lallemand, Y., and Gomez Perdiguero, E.
701 (2021). Megakaryocyte production is sustained by direct differentiation from
702 erythromyeloid progenitors in the yolk sac until midgestation. Immunity *54*, 1433-1446
703 e1435. 10.1016/j.immuni.2021.04.026.
704 16. Soares-da-Silva, F., Freyer, L., Elsaid, R., Burlen-Defranoux, O., Iturri, L., Sismeiro, O.,
705 Pinto-do, O.P., Gomez-Perdiguero, E., and Cumano, A. (2021). Yolk sac, but not
706 hematopoietic stem cell-derived progenitors, sustain erythropoiesis throughout murine
707 embryonic life. J Exp Med *218*. 10.1084/jem.20201729.
708 17. de Bruijn, M.F., Ma, X., Robin, C., Ottersbach, K., Sanchez, M.J., and Dzierzak, E.
709 (2002). Hematopoietic stem cells localize to the endothelial cell layer in the midgestation
710 mouse aorta. Immunity *16*, 673-683. 10.1016/s1074-7613(02)00313-8.
711 18. Hadland, B.K., Varnum-Finney, B., Poulos, M.G., Moon, R.T., Butler, J.M., Rafii, S.,
712 and Bernstein, I.D. (2015). Endothelium and NOTCH specify and amplify aorta-gonad-
713 mesonephros-derived hematopoietic stem cells. J Clin Invest *125*, 2032-2045.
714 10.1172/JCI80137.
715 19. Patel, S.H., Christodoulou, C., Weinreb, C., Yu, Q., da Rocha, E.L., Pepe-Mooney, B.J.,
716 Bowling, S., Li, L., Osorio, F.G., Daley, G.Q., and Camargo, F.D. (2022). Lifelong
717 multilineage contribution by embryonic-born blood progenitors. Nature *606*, 747-753.
718 10.1038/s41586-022-04804-z.

719 20. Ding, B.S., Nolan, D.J., Butler, J.M., James, D., Babazadeh, A.O., Rosenwaks, Z., Mittal,
720 V., Kobayashi, H., Shido, K., Lyden, D., et al. (2010). Inductive angiocrine signals from
721 sinusoidal endothelium are required for liver regeneration. Nature *468*, 310-315.
722 10.1038/nature09493.
723 21. Kobayashi, H., Butler, J.M., O'Donnell, R., Kobayashi, M., Ding, B.S., Bonner, B., Chiu,
724 V.K., Nolan, D.J., Shido, K., Benjamin, L., and Rafii, S. (2010). Angiocrine factors from
725 Akt-activated endothelial cells balance self-renewal and differentiation of haematopoietic
726 stem cells. Nat Cell Biol *12*, 1046-1056. 10.1038/ncb2108.
727 22. Butler, J.M., Gars, E.J., James, D.J., Nolan, D.J., Scandura, J.M., and Rafii, S. (2012).
728 Development of a vascular niche platform for expansion of repopulating human cord
729 blood stem and progenitor cells. Blood *120*, 1344-1347. 10.1182/blood-2011-12-398115.
730 23. Yzaguirre, A.D., and Speck, N.A. (2016). Insights into blood cell formation from
731 hemogenic endothelium in lesser-known anatomic sites. Dev Dyn *245*, 1011-1028.
732 10.1002/dvdy.24430.
733 24. Zhu, Q., Gao, P., Tober, J., Bennett, L., Chen, C., Uzun, Y., Li, Y., Howell, E.D.,
734 Mumau, M., Yu, W., et al. (2020). Developmental trajectory of prehematopoietic stem
735 cell formation from endothelium. Blood *136*, 845-856. 10.1182/blood.2020004801.
736 25. North, T., Gu, T.L., Stacy, T., Wang, Q., Howard, L., Binder, M., Marin-Padilla, M., and
737 Speck, N.A. (1999). Cbfa2 is required for the formation of intra-aortic hematopoietic
738 clusters. Development *126*, 2563-2575. 10.1242/dev.126.11.2563.
739 26. Chen, M.J., Yokomizo, T., Zeigler, B.M., Dzierzak, E., and Speck, N.A. (2009). Runx1 is
740 required for the endothelial to haematopoietic cell transition but not thereafter. Nature
741 *457*, 887-891. 10.1038/nature07619.

742 27. Eliades, A., Wareing, S., Marinopoulou, E., Fadlullah, M.Z.H., Patel, R., Grabarek, J.B.,
743 Plusa, B., Lacaud, G., and Kouskoff, V. (2016). The Hemogenic Competence of
744 Endothelial Progenitors Is Restricted by Runx1 Silencing during Embryonic
745 Development. Cell Rep *15*, 2185-2199. 10.1016/j.celrep.2016.05.001.
746 28. Yzaguirre, A.D., Howell, E.D., Li, Y., Liu, Z., and Speck, N.A. (2018). Runx1 is
747 sufficient for blood cell formation from non-hemogenic endothelial cells in vivo only
748 during early embryogenesis. Development *145*, dev158162. 10.1242/dev.158162.
749 29. Lis, R., Karrasch, C.C., Poulos, M.G., Kunar, B., Redmond, D., Duran, J.G.B., Badwe,
750 C.R., Schachterle, W., Ginsberg, M., Xiang, J., et al. (2017). Conversion of adult
751 endothelium to immunocompetent haematopoietic stem cells. Nature *545*, 439-445.
752 10.1038/nature22326.
753 30. Sandler, V.M., Lis, R., Liu, Y., Kedem, A., James, D., Elemento, O., Butler, J.M.,
754 Scandura, J.M., and Rafii, S. (2014). Reprogramming human endothelial cells to
755 haematopoietic cells requires vascular induction. Nature *511*, 312-318.
756 10.1038/nature13547.
757 31. Pelosi, E., Castelli, G., Martin-Padura, I., Bordoni, V., Santoro, S., Conigliaro, A., Cerio,
758 A.M., De Santis Puzzonia, M., Marighetti, P., Biffoni, M., et al. (2012). Human haemato-
759 endothelial precursors: cord blood CD34+ cells produce haemogenic endothelium. PLoS
760 One *7*, e51109. 10.1371/journal.pone.0051109.
761 32. Kilani, B., Gourdou-Latyszenok, V., Guy, A., Bats, M.L., Peghaire, C., Parrens, M.,
762 Renault, M.A., Duplaa, C., Villeval, J.L., Rautou, P.E., et al. (2019). Comparison of
763 endothelial promoter efficiency and specificity in mice reveals a subset of Pdgfb-positive
764 hematopoietic cells. J Thromb Haemost *17*, 827-840. 10.1111/jth.14417.

765 33. Pei, W., Shang, F., Wang, X., Fanti, A.K., Greco, A., Busch, K., Klapproth, K., Zhang,
766 Q., Quedenau, C., Sauer, S., et al. (2020). Resolving Fates and Single-Cell
767 Transcriptomes of Hematopoietic Stem Cell Clones by PolyloxExpress Barcoding. Cell
768 Stem Cell *27*, 383-395 e388. 10.1016/j.stem.2020.07.018.
769 34. Hernandez, G.E., Ma, F., Martinez, G., Firozabadi, N.B., Salvador, J., Juang, L.J., Leung,
770 J., Zhao, P., Lopez, D.A., Ardehali, R., et al. (2022). Aortic intimal resident macrophages
771 are essential for maintenance of the non-thrombogenic intravascular state. Nat
772 Cardiovasc Res *1*, 67-84. 10.1038/s44161-021-00006-4.
773 35. Gentek, R., Ghigo, C., Hoeffel, G., Bulle, M.J., Msallam, R., Gautier, G., Launay, P.,
774 Chen, J., Ginhoux, F., and Bajenoff, M. (2018). Hemogenic Endothelial Fate Mapping
775 Reveals Dual Developmental Origin of Mast Cells. Immunity *48*, 1160-1171 e1165.
776 10.1016/j.immuni.2018.04.025.
777 36. Wang, L., Benedito, R., Bixel, M.G., Zeuschner, D., Stehling, M., Savendahl, L., Haigh,
778 J.J., Snippert, H., Clevers, H., Breier, G., et al. (2013). Identification of a clonally
779 expanding haematopoietic compartment in bone marrow. EMBO J *32*, 219-230.
780 10.1038/emboj.2012.308.
781 37. Sorensen, I., Adams, R.H., and Gossler, A. (2009). DLL1-mediated Notch activation
782 regulates endothelial identity in mouse fetal arteries. Blood *113*, 5680-5688.
783 10.1182/blood-2008-08-174508.
784 38. Pitulescu, M.E., Schmidt, I., Benedito, R., and Adams, R.H. (2010). Inducible gene
785 targeting in the neonatal vasculature and analysis of retinal angiogenesis in mice. Nat
786 Protoc *5*, 1518-1534. 10.1038/nprot.2010.113.

787 39. Okabe, K., Kobayashi, S., Yamada, T., Kurihara, T., Tai-Nagara, I., Miyamoto, T.,
788 Mukouyama, Y.S., Sato, T.N., Suda, T., Ema, M., and Kubota, Y. (2014). Neurons limit
789 angiogenesis by titrating VEGF in retina. Cell *159*, 584-596. 10.1016/j.cell.2014.09.025.
790 40. Alvarez-Aznar, A., Martinez-Corral, I., Daubel, N., Betsholtz, C., Makinen, T., and
791 Gaengel, K. (2020). Tamoxifen-independent recombination of reporter genes limits
792 lineage tracing and mosaic analysis using CreER(T2) lines. Transgenic Res *29*, 53-68.
793 10.1007/s11248-019-00177-8.
794 41. Stifter, S.A., and Greter, M. (2020). STOP floxing around: Specificity and leakiness of
795 inducible Cre/loxP systems. Eur J Immunol *50*, 338-341. 10.1002/eji.202048546.
796 42. Liu, Y., Suckale, J., Masjkur, J., Magro, M.G., Steffen, A., Anastassiadis, K., and
797 Solimena, M. (2010). Tamoxifen-independent recombination in the RIP-CreER mouse.
798 PLoS One *5*, e13533. 10.1371/journal.pone.0013533.
799 43. Vooijs, M., Jonkers, J., and Berns, A. (2001). A highly efficient ligand-regulated Cre
800 recombinase mouse line shows that recombination is position dependent. Embo Reports
801 *2*, 292-297. 10.1093/embo-reports/kve064.
802 44. Nakano, T. (1996). In vitro development of hematopoietic system from mouse embryonic
803 stem cells: a new approach for embryonic hematopoiesis. Int J Hematol *65*, 1-8.
804 10.1016/s0925-5710(96)00531-2.
805 45. Xu, C., Gao, X., Wei, Q., Nakahara, F., Zimmerman, S.E., Mar, J., and Frenette, P.S.
806 (2018). Stem cell factor is selectively secreted by arterial endothelial cells in bone
807 marrow. Nat Commun *9*, 2449. 10.1038/s41467-018-04726-3.

808 46. Yoder, M.C., Hiatt, K., Dutt, P., Mukherjee, P., Bodine, D.M., and Orlic, D. (1997).
809 Characterization of definitive lymphohematopoietic stem cells in the day 9 murine yolk
810 sac. Immunity *7*, 335-344. 10.1016/s1074-7613(00)80355-6.
811 47. Auffray, C., Sieweke, M.H., and Geissmann, F. (2009). Blood monocytes: development,
812 heterogeneity, and relationship with dendritic cells. Annu Rev Immunol *27*, 669-692.
813 10.1146/annurev.immunol.021908.132557.
814 48. Ghosn, E.E., Cassado, A.A., Govoni, G.R., Fukuhara, T., Yang, Y., Monack, D.M.,
815 Bortoluci, K.R., Almeida, S.R., Herzenberg, L.A., and Herzenberg, L.A. (2010). Two
816 physically, functionally, and developmentally distinct peritoneal macrophage subsets.
817 Proc Natl Acad Sci U S A *107*, 2568-2573. 10.1073/pnas.0915000107.
818 49. Kucinski, I., Campos, J., Barile, M., Severi, F., Bohin, N., Moreira, P.N., Allen, L.,
819 Lawson, H., Haltalli, M.L.R., Kinston, S.J., et al. (2024). A time- and single-cell-resolved
820 model of murine bone marrow hematopoiesis. Cell Stem Cell *31*, 244-259 e210.
821 10.1016/j.stem.2023.12.001.
822 50. Skulimowska, I., Morys, J., Sosniak, J., Gonka, M., Gulati, G., Sinha, R., Kowalski, K.,
823 Mosiolek, S., Weissman, I.L., Jozkowicz, A., et al. (2024). Polyclonal regeneration of
824 mouse bone marrow endothelial cells after irradiative conditioning. Cell Rep *43*, 114779.
825 10.1016/j.celrep.2024.114779.
826 51. Pei, W., Feyerabend, T.B., Rossler, J., Wang, X., Postrach, D., Busch, K., Rode, I.,
827 Klapproth, K., Dietlein, N., Quedenau, C., et al. (2017). Polylox barcoding reveals
828 haematopoietic stem cell fates realized in vivo. Nature *548*, 456-460.
829 10.1038/nature23653.

830 52. Pei, W., Wang, X., Rossler, J., Feyerabend, T.B., Hofer, T., and Rodewald, H.R. (2019).
831 Using Cre-recombinase-driven Polylox barcoding for in vivo fate mapping in mice. Nat
832 Protoc *14*, 1820-1840. 10.1038/s41596-019-0163-5.
833 53. Baryawno, N., Przybylski, D., Kowalczyk, M.S., Kfoury, Y., Severe, N., Gustafsson, K.,
834 Kokkaliaris, K.D., Mercier, F., Tabaka, M., Hofree, M., et al. (2019). A Cellular
835 Taxonomy of the Bone Marrow Stroma in Homeostasis and Leukemia. Cell *177*, 1915-
836 1932 e1916. 10.1016/j.cell.2019.04.040.
837 54. Tikhonova, A.N., Dolgalev, I., Hu, H., Sivaraj, K.K., Hoxha, E., Cuesta-Dominguez, A.,
838 Pinho, S., Akhmetzyanova, I., Gao, J., Witkowski, M., et al. (2019). The bone marrow
839 microenvironment at single-cell resolution. Nature *569*, 222-228. 10.1038/s41586-019-
840 1104-8.
841 55. Baccin, C., Al-Sabah, J., Velten, L., Helbling, P.M., Grunschlager, F., Hernandez-
842 Malmierca, P., Nombela-Arrieta, C., Steinmetz, L.M., Trumpp, A., and Haas, S. (2020).
843 Combined single-cell and spatial transcriptomics reveal the molecular, cellular and
844 spatial bone marrow niche organization. Nat Cell Biol *22*, 38-48. 10.1038/s41556-019-
845 0439-6.
846 56. Sivaraj, K.K., Jeong, H.W., Dharmalingam, B., Zeuschner, D., Adams, S., Potente, M.,
847 and Adams, R.H. (2021). Regional specialization and fate specification of bone stromal
848 cells in skeletal development. Cell Rep *36*, 109352. 10.1016/j.celrep.2021.109352.
849 57. Zhong, L., Yao, L., Tower, R.J., Wei, Y., Miao, Z., Park, J., Shrestha, R., Wang, L., Yu,
850 W., Holdreith, N., et al. (2020). Single cell transcriptomics identifies a unique adipose
851 lineage cell population that regulates bone marrow environment. Elife *9*, e54695.
852 10.7554/eLife.54695.

853 58. Lang, A., Collins, J.M., Nijsure, M.P., Belali, S., Khan, M.P., Moharrer, Y., Schipani, E.,
854 Yien, Y.Y., Fan, Y., Gelinsky, M., et al. (2025). Local erythropoiesis directs oxygen
855 availability in bone fracture repair. bioRxiv, 2025.2001. 2010.632440.
856 10.1101/2025.01.10.632440.
857 59. Smith, N.P., Janton, C., Alcantara, A.C.M., George, M., Mankongtreecheep, K., Mao, G.,
858 Villani, A.-C., and Kronenberg, H.M. (2025). Single cell RNA sequencing shows that
859 cells expressing Sox9 postnatally populate most skeletal lineages in mouse bone. Journal
860 of Bone and Mineral Research, zjaf043.
861 60. Howell, E.D., Yzaguirre, A.D., Gao, P., Lis, R., He, B., Lakadamyali, M., Rafii, S., Tan,
862 K., and Speck, N.A. (2021). Efficient hemogenic endothelial cell specification by
863 RUNX1 is dependent on baseline chromatin accessibility of RUNX1-regulated TGFβ
864 target genes. Genes & Development *35*, 1475-1489. 10.1101/gad.348738.121.
865 61. Serina Secanechia, Y.N., Bergiers, I., Rogon, M., Arnold, C., Descostes, N., Le, S.,
866 Lopez-Anguita, N., Ganter, K., Kapsali, C., Bouilleau, L., et al. (2022). Identifying a
867 novel role for the master regulator Tal1 in the Endothelial to Hematopoietic Transition.
868 Sci Rep *12*, 16974. 10.1038/s41598-022-20906-0.
869 62. Bergiers, I., Andrews, T., Vargel Bolukbasi, O., Buness, A., Janosz, E., Lopez-Anguita,
870 N., Ganter, K., Kosim, K., Celen, C., Itir Percin, G., et al. (2018). Single-cell
871 transcriptomics reveals a new dynamical function of transcription factors during
872 embryonic hematopoiesis. Elife *7*, e29312. 10.7554/eLife.29312.
873 63. Guibentif, C., Ronn, R.E., Boiers, C., Lang, S., Saxena, S., Soneji, S., Enver, T.,
874 Karlsson, G., and Woods, N.B. (2017). Single-Cell Analysis Identifies Distinct Stages of

875 Human Endothelial-to-Hematopoietic Transition. Cell Rep *19*, 10-19.
876 10.1016/j.celrep.2017.03.023.
877 64. Wilson, N.K., Foster, S.D., Wang, X., Knezevic, K., Schutte, J., Kaimakis, P., Chilarska,
878 P.M., Kinston, S., Ouwehand, W.H., Dzierzak, E., et al. (2010). Combinatorial
879 transcriptional control in blood stem/progenitor cells: genome-wide analysis of ten major
880 transcriptional regulators. Cell Stem Cell *7*, 532-544. 10.1016/j.stem.2010.07.016.
881 65. Kalucka, J., de Rooij, L., Goveia, J., Rohlenova, K., Dumas, S.J., Meta, E., Conchinha,
882 N.V., Taverna, F., Teuwen, L.A., Veys, K., et al. (2020). Single-Cell Transcriptome Atlas
883 of Murine Endothelial Cells. Cell *180*, 764-779 e720. 10.1016/j.cell.2020.01.015.
884 66. Qi, L., Huang, C., Wu, X., Tao, Y., Yan, J., Shi, T., Cao, C., Han, L., Qiu, M., Ma, Q., et
885 al. (2017). Hierarchical Specification of Pruriceptors by Runt-Domain Transcription
886 Factor Runx1. J Neurosci *37*, 5549-5561. 10.1523/JNEUROSCI.0094-17.2017.
887 67. Yvernogeau, L., Gautier, R., Petit, L., Khoury, H., Relaix, F., Ribes, V., Sang, H.,
888 Charbord, P., Souyri, M., Robin, C., and Jaffredo, T. (2019). In vivo generation of
889 haematopoietic stem/progenitor cells from bone marrow-derived haemogenic
890 endothelium. Nat Cell Biol *21*, 1334-1345. 10.1038/s41556-019-0410-6.
891 68. Richard, C., Drevon, C., Canto, P.Y., Villain, G., Bollerot, K., Lempereur, A., Teillet,
892 M.A., Vincent, C., Rossello Castillo, C., Torres, M., et al. (2013). Endothelio-
893 mesenchymal interaction controls runx1 expression and modulates the notch pathway to
894 initiate aortic hematopoiesis. Dev Cell *24*, 600-611. 10.1016/j.devcel.2013.02.011.
895 69. Dignum, T., Varnum-Finney, B., Srivatsan, S.R., Dozono, S., Waltner, O., Heck, A.M.,
896 Ishida, T., Nourigat-McKay, C., Jackson, D.L., Rafii, S., et al. (2021). Multipotent

897 progenitors and hematopoietic stem cells arise independently from hemogenic
898 endothelium in the mouse embryo. Cell Rep *36*, 109675. 10.1016/j.celrep.2021.109675.
899 70. Ambler, C.A., Nowicki, J.L., Burke, A.C., and Bautch, V.L. (2001). Assembly of trunk
900 and limb blood vessels involves extensive migration and vasculogenesis of somite-
901 derived angioblasts. Dev Biol *234*, 352-364. 10.1006/dbio.2001.0267.
902 71. Pudliszewski, M., and Pardanaud, L. (2005). Vasculogenesis and angiogenesis in the
903 mouse embryo studied using quail/mouse chimeras. Int J Dev Biol *49*, 355-361.
904 10.1387/ijdb.041956mp.
905 72. Pardanaud, L., and Dieterlen-Lievre, F. (1999). Manipulation of the
906 angiopoietic/hemangiopoietic commitment in the avian embryo. Development *126*, 617-
907 627. 10.1242/dev.126.4.617.
908 73. Qiu, J., Fan, X., Wang, Y., Jin, H., Song, Y., Han, Y., Huang, S., Meng, Y., Tang, F., and
909 Meng, A. (2016). Embryonic hematopoiesis in vertebrate somites gives rise to definitive
910 hematopoietic stem cells. J Mol Cell Biol *8*, 288-301. 10.1093/jmcb/mjw024.
911 74. Nguyen, P.D., Hollway, G.E., Sonntag, C., Miles, L.B., Hall, T.E., Berger, S., Fernandez,
912 K.J., Gurevich, D.B., Cole, N.J., Alaei, S., et al. (2014). Haematopoietic stem cell
913 induction by somite-derived endothelial cells controlled by meox1. Nature *512*, 314-318.
914 10.1038/nature13678.
915 75. Morikawa, S., Mabuchi, Y., Niibe, K., Suzuki, S., Nagoshi, N., Sunabori, T., Shimmura,
916 S., Nagai, Y., Nakagawa, T., Okano, H., and Matsuzaki, Y. (2009). Development of
917 mesenchymal stem cells partially originate from the neural crest. Biochem Biophys Res
918 Commun *379*, 1114-1119. 10.1016/j.bbrc.2009.01.031.

919 76. Takashima, Y., Era, T., Nakao, K., Kondo, S., Kasuga, M., Smith, A.G., and Nishikawa,
920 S. (2007). Neuroepithelial cells supply an initial transient wave of MSC differentiation.
921 Cell *129*, 1377-1388. 10.1016/j.cell.2007.04.028.
922 77. Vodyanik, M.A., Yu, J., Zhang, X., Tian, S., Stewart, R., Thomson, J.A., and Slukvin, II
923 (2010). A mesoderm-derived precursor for mesenchymal stem and endothelial cells. Cell
924 Stem Cell *7*, 718-729. 10.1016/j.stem.2010.11.011.
925 78. Bianco, P., Robey, P.G., and Simmons, P.J. (2008). Mesenchymal stem cells: revisiting
926 history, concepts, and assays. Cell Stem Cell *2*, 313-319. 10.1016/j.stem.2008.03.002.
927 79. Oswald, J., Boxberger, S., Jorgensen, B., Feldmann, S., Ehninger, G., Bornhauser, M.,
928 and Werner, C. (2004). Mesenchymal stem cells can be differentiated into endothelial
929 cells in vitro. Stem Cells *22*, 377-384. 10.1634/stemcells.22-3-377.
930 80. Conrad, C., Niess, H., Huss, R., Huber, S., von Luettichau, I., Nelson, P.J., Ott, H.C.,
931 Jauch, K.W., and Bruns, C.J. (2009). Multipotent mesenchymal stem cells acquire a
932 lymphendothelial phenotype and enhance lymphatic regeneration in vivo. Circulation
933 *119*, 281-289. 10.1161/CIRCULATIONAHA.108.793208.
934 81. Ubil, E., Duan, J., Pillai, I.C., Rosa-Garrido, M., Wu, Y., Bargiacchi, F., Lu, Y.,
935 Stanbouly, S., Huang, J., Rojas, M., et al. (2014). Mesenchymal-endothelial transition
936 contributes to cardiac neovascularization. Nature *514*, 585-590. 10.1038/nature13839.
937 82. Crisan, M. (2013). Transition of mesenchymal stem/stromal cells to endothelial cells.
938 Stem Cell Res Ther *4*, 95. 10.1186/scrt306.
939 83. Xu, Y., and Kovacic, J.C. (2023). Endothelial to Mesenchymal Transition in Health and
940 Disease. Annu Rev Physiol *85*, 245-267. 10.1146/annurev-physiol-032222-080806.

941 84. Termini, C.M., Pang, A., Fang, T., Roos, M., Chang, V.Y., Zhang, Y., Setiawan, N.J.,
942 Signaevskaia, L., Li, M., Kim, M.M., et al. (2021). Neuropilin 1 regulates bone marrow
943 vascular regeneration and hematopoietic reconstitution. Nat Commun *12*, 6990.
944 10.1038/s41467-021-27263-y.
945 85. Zheng, B., Zhang, Z., Black, C.M., de Crombrugghe, B., and Denton, C.P. (2002).
946 Ligand-dependent genetic recombination in fibroblasts : a potentially powerful technique
947 for investigating gene function in fibrosis. Am J Pathol *160*, 1609-1617. 10.1016/S0002-
948 9440(10)61108-X.
949 86. Madisen, L., Zwingman, T.A., Sunkin, S.M., Oh, S.W., Zariwala, H.A., Gu, H., Ng, L.L.,
950 Palmiter, R.D., Hawrylycz, M.J., Jones, A.R., et al. (2010). A robust and high-throughput
951 Cre reporting and characterization system for the whole mouse brain. Nat Neurosci *13*,
952 133-140. 10.1038/nn.2467.
953 87. Muzumdar, M.D., Tasic, B., Miyamichi, K., Li, L., and Luo, L. (2007). A global double-
954 fluorescent Cre reporter mouse. Genesis *45*, 593-605. 10.1002/dvg.20335.
955 88. Happerfield, L., Saward, R., Grimwade, L., Bloxham, D., and Erber, W. (2008).
956 Automated immunostaining of cell smears: an alternative to flow cytometry8.
957 International Journal of Laboratory Hematology *30*, 8.
958

959 **METHODS**

960 **RESOURCES TABLE**

REAGENT or RESOURCE	SOURCE	IDENTIFIER
Antibodies		

BD Horizon™ BV786 Rat Anti-Mouse CD117	BD Biosciences	564012; RRID:AB_2732005
Brilliant Violet 421™ anti-mouse CD117 (c-Kit) Antibody	BioLegend	105828; RRID:AB_11204256
Brilliant Violet 785™ anti-mouse CD117 (c-Kit) Antibody	BioLegend	105841; RRID:AB_2629799
BD Pharmingen™ APC Rat Anti-CD11b	BD Biosciences	553312; RRID:AB_398535
PerCP/Cyanine5.5 anti-mouse CD150 (SLAM) Antibody	BioLegend	115922; RRID:AB_2303663
APC/Fire™ 750 anti-mouse CD150 (SLAM) Antibody	BioLegend	115940; RRID:AB_2629587
BD Pharmingen™ APC-Cy™7 Rat Anti-Mouse CD19	BD Biosciences	557655; RRID:AB_396770
BD Horizon™ BUV737 Rat Anti-Mouse CD19	BD Biosciences	612781; RRID:AB_2870110
Brilliant Violet 510™ anti-mouse CD3 Antibody	BioLegend	100234; RRID:AB_2562555
BD Pharmingen™ Purified Rat Anti-Mouse CD31	BD Biosciences	553370; RRID:AB_394816
BV421 anti-mouse Cd31	BD Biosciences	563356; RRID:AB_2738154
Brilliant Violet 421™ anti-mouse CD31 Antibody	BioLegend	102424; RRID:AB_2650892
Brilliant Violet 605™ anti-mouse CD31 Antibody	BioLegend	102427; RRID:AB_2563982
BD Pharmingen™ Alexa Fluor® 700 Rat Anti-Mouse CD45	BD Biosciences	560510; RRID:AB_1645208
BD OptiBuild™ BUV615 Rat Anti-Mouse CD45	BD Biosciences	751170; RRID:AB_2875194
PE anti-mouse CD45 Antibody	BioLegend	103106; RRID:AB_312971
PerCP/Cyanine5.5 anti-mouse CD45 Antibody	BioLegend	103131; RRID:AB_893344 103132; RRID:AB_893340
BD Horizon™ BV510 Hamster Anti-Mouse CD48	BD Biosciences	563536; RRID:AB_2738266
APC/Cyanine7 anti-mouse CD48 Antibody	BioLegend	103432; RRID:AB_2561463
Brilliant Violet 510™ anti-mouse CD48 Antibody	BioLegend	103443; RRID:AB_2650826
Collagen I Polyclonal Antibody, Biotin	Invitrogen	PA1-28530; RRID: AB_1956957
Endomucin Monoclonal Antibody (eBioV.7C7 (V.7C7)), eFluor™ 660	Invitrogen	50-5851-82; RRID:AB_11220465
Anti-Endomucin Antibody (V.7C7) AF546	Santa Cruz Biotechnology	sc-65495 AF546; RRID:AB_2100037
BD Pharmingen™ PE-Cy™7 Rat Anti-Mouse Ly-6G	BD Biosciences	560601; RRID:AB_1727562
BD Horizon™ BUV395 Rat Anti-Mouse Ly-6G	BD Biosciences	563978; RRID:AB_2716852
BD Pharmingen™ APC Mouse Lineage Antibody Cocktail, with Isotype Control	BD Biosciences	558074; RRID:AB_1645213

Goat anti-Rat IgG (H+L) Highly Cross-Adsorbed Secondary Antibody, Alexa Fluor™ Plus 594	Invitrogen	A48264; RRID:AB_2896333
RUNX1 Monoclonal Antibody (RXDMC), PE, eBioscience™	Invitrogen	12-9816-80; RRID:AB_11151519
BD Pharmingen™ PE-Cy™7 Rat Anti-Mouse Ly-6A/E	BD Biosciences	561021; RRID:AB_2034021
PE/Cy7 anti-mouse Ly-6A/E (Sca-1)	BioLegend	108114; RRID:AB_493596
PerCP/Cyanine5.5 anti-mouse TER-119/Erythroid Cells Antibody	BioLegend	116228; RRID:AB_893636
Brilliant Violet 605™ anti-mouse TER-119/Erythroid Cells Antibody	BioLegend	116239; RRID:AB_2562447
BD Pharmingen™ Alexa Fluor® 647 Rat Anti-Mouse CD144	BD Biosciences	562242; RRID:AB_2737608
BD Pharmingen™ PE Rat Anti-Mouse CD144	BD Biosciences	562243; RRID:AB_2737609
BUV737 Rat Anti-Mouse CD144	BD Biosciences	741792; RRID:AB_2871138
Alexa Fluor® 647 anti-mouse CD144 (VE-cadherin) Antibody	BioLegend	138006; RRID:AB_10569114
BD OptiBuild™ RB780 Rat Anti-Mouse CD144	BD Biosciences	755945; RRID:AB_3683567
PE anti-mouse CD144 (VE-cadherin) Antibody	BioLegend	138010; RRID:AB_10641139
PE/Cyanine7 anti-mouse CD144 (VE-cadherin) Antibody	BioLegend	138015; RRID:AB_2562885 138016; RRID:AB_2562886
PE anti-mouse CD144 (VE-cadherin) Antibody	BioLegend	138105; RRID:AB_2077941
Chemicals, peptides, and recombinant proteins		
5-FLUOROURACIL	Sigma-Aldrich	F6627
7-AAD Viability Stain SOLN	Life Technologies Corp.	00-6993-50
7-Aminoactinomycin D	Sigma-Aldrich	A9400
ACETONE	MALLINCKRODT	2440
ACK lysing Buffer	Lonza	10-548E
Acrylamide/Bis 19:1, 40% (w/v) solution	Invitrogen	AM9024
Acrylamide/Bis-acrylamide 19:1	Sigma-Aldrich	A2917
Acridine Orange / Propidium Iodide Stain	Logos Biosystems	F23001
AMPure beads	Beckman Coulter	A63881
Antibiotic-Antimycotic	Gibco	15240062

Anti-Rat Ig, κ/Negative Control (BSA) Compensation Plus (7.5 μm) Particles Set	BD Biosciences	560499
Anti-Rat Ig, κ/Negative Control Compensation Particles Set	BD Biosciences	552844
APC/Fire™ 750 Streptavidin	BioLegend	405250
Azide-Free Fc Receptor Blocker	INNOVEX	NB335-60
Bovine Serum Albumin solution	MP Biomedicals	160069
CellROX Orange Flow Cytometry Assay Kit	Invitrogen	C10493
Collagenase Type 2	Worthington Biochemical Corporation	LS004176
Dispase	Worthington Biomedical	LS02109
Deoxyribonuclease	Worthington Biomedical	LS006344
DAPI (4',6-Diamidino-2-Phenylindole, Dilactate)	BioLegend	422801
Dihydroethidium (Hydroethidine)	Invitrogen	D1168
Donkey serum	Sigma-Aldrich	D9663
DRAQ5	Biostatus	DR50200
EDTA (0.5M, pH 8.0)	KD Medical	RGF3130
ETHYL ALCOHOL (200 PROOF ANHYDROUS)	Warner-Graham Co.	201096
Ethylenediamine-N,N,N′,N′-tetra-2-propanol	Sigma-Aldrich	8219401000
Fetal Bovine Serum	Millipore Sigma	F2442-500ML (Lot 24G002)
Fc Receptor Blocker	Innovex	NB309-30
Formalin solution, neutral buffered, 10%	Sigma-Aldrich	HT501128-4L
Gelatin	Sigma-Aldrich	G9391
Goldenrod™ Animal Lancet	Braintree Scientific Inc.	GR-3MM
HBSS	Gibco	14025075
HEPES	Gibco	15630080
Immu-Mount™ mountant	Epredia	9990402
Isoflurane	Baxter	10019036040
Mag-Bind® TotalPure NGS	Omega Bio-tek	M1378-01
Methanol, HPLC Grade	Avantor	JT-9093-03
MojoSort™ Mouse CD45 Nanobeads	BioLegend	480028
Kwik Stop® Stypic Power	Miracle Care	SKU 423615
Lineage Cell Depletion Kit, mouse	MiltenyiBiotec	130-090-858
Lipopolysaccharides	Sigma Aldrich	L2880-25MG
Microscope Slides	MATSUNAMI GLASS IND.	SUMGP12

Neutral Protease, Partially Purified, Animal Free/AF	Worthington Biochemical Corporation	LS02109
Paraformaldehyde (formaldehyde) aqueous solution (20%)	Electron Microscopy Sciences	15713-S
Penicillin-Streptomycin	Gibco	15140-122
Peanut oil	Sigma-Aldrich	P2144
Phusion Green Hot Start II High-Fidelity PCR Master Mix	Thermo Scientific	F566L
pHrodo™ Red E. coli BioParticles	Invitrogen	P35361
Polyvinylpyrrolidone	Sigma-Aldrich	P5288
Propidium iodide	Sigma-Aldrich	P4170
Q5 Hot Start High-Fidelity 2X Master Mix	NEB	M0494S
Richard-Allan Scientific™ Cover glass	Epredia	102424
RNeasy® Micro Kit	QIAGEN	74004
Saponin	Sigma-Aldrich	47036
SPRIselect Beads	Beckman Coulter	B23318
Sucrose	Sigma-Aldrich	S8501
SuperScript™ IV First-Strand Synthesis System	Invitrogen	18091050
Tamoxifen	Sigma-Aldrich	T5648
TaqMan™ Fast Advanced Master Mix	ThermoFisher Scientific	4444557
Thioglycollate Broth	Sigma Aldrich	70157
Tissue-Tek® O.C.T. Compound	SAKURA	4583
Triton™ X-100	Sigma-Aldrich	T9284
Trypsin-EDTA (0.25%), phenol red	Gibco	25200056
TruBond™ 380 Adhesion Slide	Electron Microscopy Sciences	63700-Y10
UNI-TRIEVE	INNOVEX	NB325
VA-044 (Water soluble Azo initiators)	FUJIFILM Labchem Wako	VA-044
VECTASHIELD Vibrance Antifade Mounting Medium	Vector Laboratories	H-1700-10
Zombie Aqua™ Fixable Viability Kit	BioLegend	423101
Zombie NIR™ Fixable Viability Kit	BioLegend	423105
Zombie UV™ Fixable Viability Kit	BioLegend	423107
Zombie Yellow™ Fixable Viability Kit	BioLegend	423103
Zymosan A from Saccharomyces cerevisiae	Sigma Aldrich	Z4250
Critical commercial assays		

Chromium GEM-X Single Cell 3' Kit	10× Genomics	1000686
Chromium GEM-X Single Cell 3' Chip Kit v4	10× Genomics	1000690
Chromium Next GEM Chip G Single Cell Kit	10× Genomics	1000127
Chromium Next GEM Single Cell 3' Kit v3.1	10× Genomics	1000269
Dual Index Kit TT Set	10× Genomics	1000215
NextSeq 2000 P4 Reagents (100 Cycles)	Illumina	20100994
NextSeq 2000 P3 Reagents (100 Cycles)	Illumina	20040559
Deposited data		
Polylox PacBio long-read sequencing data	This Study	PRJNA1079369
Single cell RNA seq data	This Study	PRJNA1079369
Experimental models: Cell lines		
OP9 cells	Dr. Nakano; same line deposited in ATCC	ATCC # CRL-2749; RRID:CVCL_4398
Experimental models: Organisms/strains		
Cdh5-Cre(PAC)^{ERT2}	Drs. R. Adams and M. Boehm; also available from Taconic Biosciences	MGI:3848982 Taconic # 13073
Cdh5-Cre(BAC)^{ERT2}	Drs. Y. Kubota and Y. Mukoyama	MGI:5705396
Col1a2-CreERT	JAX, #029567	MGI:3785760
ZsGreen (Ai6)	JAX, #007906	MGI:3809522
mTmG	JAX, #007676	MGI:3716464
PolyloxExpress	Drs. H. Rodewald and A. Bhandoola	MGI:6470648
Runx1Knock-In	Drs. Q. Ma and N. Speck	MGI:7490340
Oligonucleotides		
mTmG mouse strain genotyping primers (5' – 3')	CTT TAA GCC TGC CCA GAA GA TAG AGC TTG CGG AAC CCT TC AGG GAG CTG CAG TGG AGT AG	JAX: 007676

ZsGreen mouse strain genotyping primers (5' – 3')	AAG GGA GCT GCA GTG GAG TA CCG AAA ATC TGT GGG AAG TC GGC ATT AAA GCA GCG TAT CC AAC CAG AAG TGG CAC CTG AC	JAX: 007906
Cdh5-Cre^{ERT2}(PAC) mouse strain genotyping primers (5' – 3')	TCC TGA TGG TGC CTA TCC TC CCT GTT TTG CAC GTT CAC CG CAC CCT GTT CTT TGC CTC CT	This study.
Cdh5-Cre^{ERT2}(BAC) mouse strain genotyping primers (5' – 3')	ATA CCG GAG ATC ATG CAA GC ATG TGA ACC AGC TCC CTG TC CTA GGC CAC AGA ATT GAA AGA TCT GTA GGT GGA AAT TCT AGC ATC ATC C	JAX: Protocol 029211
Col1a2-Cre^{ERT} mouse strain genotyping primers (5' – 3')	CAT GTC CAT CAG GTT CTT GC TGA AAA AGT CCA CTA ATT AAA ACC A CTA ACA ACC CTT TCT CTC AAG GT CAG GAG GTT TCG ACT AAG TTG G	JAX: Protocol 19893
Runx1 Knock-In mouse strain genotyping primers (5' – 3')	GAG TTC TCT GCT GCC TCC TGG CGA GGG CAG CCA TAG CAA CTC CGA GGC GGA TCA CAA GCA ATA	Qi, et al., 2017
PolyloxExpress mouse strain genotyping primers (5' – 3')	AAG GGA GCT GCA GTG GAG TA TAA GCC TGC CCA GAA GAC TCC AAG ACC GCG AAG AGT TTG TCC	Pei, et al., 2020
Software and algorithms		
FlowJo v10	BD	https://www.flowjo.com RRID:SCR_008520
GraphPad Prism 10	Dotmatics	www.graphpad.com RRID:SCR_002798
Snakemake	Köster et al.	https://snakemake.github.io/ RRID:SCR_003475
Lima	PacBio	https://lima.how/ RRID:SCR_025520

Iso-Seq	PacBio	https://isoseq.how/ RRID:SCR_025481
Minimap2	Li, et al (2021)	https://github.com/lh3/minimap2 RRID:SCR_018550
Cell Ranger	10x Genomics	V8.0.1, RRID:SCR_017344
Polylox barcode recovery	This study	https://github.com/CCRSF-IFX/SF_Polylox-BC
pGen calculation	Pei, et al. (2020)	https://github.com/hoefer-lab/polylox
Scanpy	Scanpy Community	https://scanpy.readthedocs.io RRID:SCR_018139
rapids-singlecell	Rapids-SingleCell	https://rapids-singlecell.readthedocs.io
decoupler	Badia-i-Mompel et al. (2022)	https://decoupler-py.readthedocs.io
scANVI	Gayoso et al. (2022)	https://github.com/scverse/scvi-tools
CellTypist	Xu et al. (2021)	https://celltypist.readthedocs.io/
Other		
Primaria™ dishes/flasks	Corning	353808; 353810; 353846
Regular Cell Culture Flask	Corning	430641U

EXPERIMENTAL MODEL AND STUDY PARTICIPANT DETAILS

Mouse strains

All animal studies were approved by the Institutional Animal Care and Use Committee of the CCR (Bethesda, MD), National Cancer Institute (NCI), NIH and conducted in adherence to the NIH Guide for the Care and Use of Laboratory Animals (National Academies Press, 2011) and approved protocols. *Cdh5-Cre^{ERT2}(PAC)* mice [37] (MGI:3848982) were a gift from Dr. R. Adams and *Cdh5-Cre^{ERT2}(BAC)* mice [39] (MGI:5705396) were a gift from Dr. Kubota. *Col1a2-CreER*

968 mice [85] were purchased from the Jackson Laboratory (JAX#029567). Cre-dependent *Ai6-*
969 *ZsGreen* [86] (JAX#007906) and *mTmG* [87] (JAX#007676) fluorescent reporter mice were
970 purchased from the Jackson Laboratory. In *ZsGreen* reporter mice, Cre activity leads to
971 constitutive expression of ZsGreen1 in cell bodies. In *mTmG* reporter mice, Cre activity leads to
972 an irreversible switch from cell membrane-localized tdTomato (mT) to membrane-localized
973 EGFP (mG). *PolyloxExpress* mice [33] were a kind gift of Drs. Hans-Reimer Rodewald and
974 Avinash Bhandoola. The Cdh5-Cre^{ERT2}/ZsGreen/*PolyloxExpress* mouse line was generated in
975 house. Runx1 conditional knock-in mice[66] (Gt(ROSA)26Sor$^{tm1(CAG\text{-}Runx1)Lzjg}$, MGI:7490340)
976 were generously provided by Drs. Qiufu Ma and Nancy Speck. Runx1 endothelial-specific
977 knock-in (*Runx1$^{EC\text{-}KI}$*) mice were generated by crossing *Runx1$^{Ki/+}$* mice with *Cdh5-*
978 *Cre^{ERT2}(PAC)/ZsGreen$^{Tg/Tg}$* mice. Upon tamoxifen treatment, Cre-mediated excision of the two
979 floxed STOP codons enables co-expression of Runx1 and ZsGreen in ECs.
980
981 All animals were bred in the animal facilities of CCR/NCI (Bethesda, MD). The mice were
982 maintained in a C57BL/6J background. Mice were identified with ear tags and routinely
983 genotyped by PCR. No mouse was excluded from the experiments, unless assessed as sick by the
984 veterinarians or fight wounds were observed at harvest. Tamoxifen (Sigma-Aldrich, #T5648)
985 dissolved in peanut oil (Sigma-Aldrich, #P2144) (10 mg·mL^{-1}) was administered orally (via
986 gavage using 22g feeding needles) at 100 mg·kg^{-1}. Unless otherwise specified, three doses on
987 consecutive days were administered. Unless indicated otherwise, 8- to 12-week-old male and
988 female mice were used when tamoxifen was administrated. No randomization or blinding was
989 used to allocate experimental groups. Mice were typically sacrificed between 9 AM and 11 AM
990 local time.

991 # METHOD DETAILS

992 **OP9 cell culture**

993 OP9 cells, a gift from Dr. T. Nakano[44] (also available from ATCC, #CRL-2749), were
994 maintained in α-MEM (Gibco #12561056; without ribonucleosides and deoxyribonucleosides,
995 with 2.2 g/L sodium bicarbonate) supplemented with 20% fetal bovine serum (FBS; Sigma-
996 Aldrich #2442). Culture dishes and flasks (Corning #353003, #430641U) were precoated with
997 gelatin (Sigma-Aldrich #G9391; ~100 µL/cm², 60 minutes at 37°C). Cells were incubated at
998 37°C in a humidified atmosphere of 95% air and 5% CO_2.

999

1000 **Bone marrow cell harvesting, culture and terminal harvest for analysis**

1001 To harvest BM cells to be cultured, mice were euthanized by cervical dislocation and soaked in
1002 70% ethanol for 5 minutes. Long bones (femurs and tibiae) were dissected, and surrounding skin,
1003 muscle, and connective tissue were carefully removed. Cleaned bones were immediately
1004 transferred into ice-cold sterile PBS and kept on ice. Once all bones were harvested, they were
1005 soaked in 70% ethanol for 1 minute and rinsed three times with ice-cold PBS.
1006 Each bone was cut into two pieces using sterile scissors and placed--with the open end facing
1007 downward-- into a sterile 500 µL microcentrifuge tube pre-perforated with a 16G needle
1008 (sterilized in advance). Each 500 µL tube was loaded with two femurs and two tibiae. To each
1009 tube, 200 µL of DMEM supplemented with 1 mM EDTA was added. The 500 µL tubes were
1010 then placed inside sterile 1.5 mL microcentrifuge tubes, sealed with Parafilm, and centrifuged at
1011 12,000 rpm for 20 seconds. The inner tubes were discarded, and the BM pellet collected in the
1012 1.5 mL tubes was resuspended in 1 mL DMEM + 1 mM EDTA.

1013 Cells were filtered through 70 µm cell strainers, centrifuged at 350 × g for 5 minutes at 4°C, and
1014 resuspended in complete DMEM (DMEM containing 15% FBS (Sigma-Aldrich #2442-500ML,
1015 LOT:24G002), Penicillin-Streptomycin [Gibco #15140-122], and Anti-Anti [Gibco #15240-
1016 062]). A single-cell suspension was prepared by pipetting 30 times with a 1 mL pipette.
1017 Bone marrow cells were cultured either on Corning Primaria™ dishes/flasks (Corning #353808,
1018 #353810, #353846) or on OP9 stromal cell monolayers in standard tissue culture dishes/flasks
1019 (Corning #353003, #430641U) precoated with gelatin (Sigma-Aldrich #G9391; ~100 µL/cm²,
1020 incubated 60 min at 37°C).
1021 Cells were seeded at a density equivalent to BM cells from two femurs and two tibiae per ~75
1022 cm² culture surface (e.g., T75 flask) in 15 mL complete DMEM. After ~32 hours, non-adherent
1023 cells and medium were removed, and adherent cells were gently washed three times with PBS.
1024 For Primaria cultures, 15 mL fresh complete DMEM was replenished twice weekly. For OP9 co-
1025 cultures, non-adherent cells and medium were removed twice weekly and replaced with fresh
1026 complete DMEM supplemented with freshly isolated unfractionated WT BM cells (from two
1027 femurs and two tibiae per ~75 cm² surface, using the same BM isolation method mentioned
1028 above).
1029 For terminal collection, at the start of the final culture week, all non-adherent cells were
1030 removed, and adherent cells were washed three times with PBS. Fresh complete DMEM (15 mL)
1031 was added. After three days, a second 15 mL complete DMEM addition was made. No further
1032 medium changes occurred before harvest. For final collection, non-adherent cells and
1033 supernatant were collected first. Adherent cells were washed with PBS, and the wash was pooled
1034 with the supernatant. Remaining adherent cells (including OP9 and BM-derived cells) were
1035 detached using 0.25% Trypsin-EDTA (Gibco #25200-056) for 5 minutes at 37°C and added to

1036 the pooled suspension. After another PBS wash, a second trypsinization (10 minutes at 37°C)
1037 was performed. All collected material from each step was combined for downstream flow
1038 cytometric analysis. For transplantation experiments, only non-adherent cells (with supernatant)
1039 and loosely adherent cells recovered after the initial 5-minute Trypsin-EDTA incubation were
1040 pooled and subjected to FACS sorting to isolate ZsGreen^{+} cells for injection.
1041
1042 **Blood collection**
1043 For terminal collection, blood was obtained from the mouse abdominal aorta with BD
1044 Vacutainer™ EDTA tubes (BD #367856) and Vaculet™ blood collection needles (23G,
1045 EXELINT #26766). Blood smears were prepared with 10 µL of collected blood. For flow
1046 cytometry analysis, ACK buffer (Lonza, #BP10-548E) was added to the blood to lyse red blood
1047 cells before Fc receptor blocking and antibody staining. For non-terminal blood collection, ~20-
1048 50µL blood was collected by submandibular blood sampling, using a 3mm animal lancet
1049 (BRAINTREE SCI., GR-3MM) and a 250µL BD Microtainer® K2EDTA tube (BD #365974).
1050 Kwik Stop® Styptic Powder was applied to stop the bleeding (Miracle Corp. #423615). For long-
1051 term, repeated blood collection, 2 drops of blood were collected from the tail vein with
1052 Microhematocrit Capillary Tubes (Fisherbrand # 22-362574). White blood cell (WBC) counts
1053 were determined using acridine orange/propidium iodide (AO/PI, Logos Biosystems, #F23001)
1054 staining and quantified with a LUNA-FL™ fluorescence cell counter (Logos Biosystems). For
1055 flow cytometry detection of ZsGreen/EGFP positive PBMCs, blood was collected with one of
1056 the methods above. For flow cytometric detection of ZsGreen^{+}/EGFP^{+} PBMCs, blood was
1057 collected using one of the three methods described above. Red blood cells were lysed with ACK
1058 buffer, and DAPI and DRAQ5 were used to exclude dead cells and to identify nucleated PBMCs.

1059

1060 **Bone marrow harvest for flow cytometry analysis**

1061 For flow cytometry analysis, bone marrow was harvested using one of the two methods
1062 described below. For hematopoietic cell isolation, bone marrow was harvested by flushing
1063 femurs and tibiae with ice-cold Sort Buffer (1× PBS [Gibco, #10010-031] supplemented with 5
1064 mM EDTA, 25 mM HEPES, and 2% FBS [Sigma-Aldrich, #F2442]). Red blood cells were then
1065 lysed using ACK lysing buffer (Lonza, #10-548E) according to the manufacturer's instructions.
1066 Cells were then washed with Sort Buffer and passed through a 40μm cell strainer (GREINER
1067 BIO-ONE, #542040, #542140). For greater preservation of endothelial cells, bone marrows were
1068 harvested by gently crushing mouse femurs and tibiae in Sort Buffer (5mM EDTA, 25mM
1069 HEPES, 2% FBS in 1× PBS). Red cell lysis was performed using ACK buffer. Bone marrow
1070 cells were then incubated with $0.1U{\cdot}mL^{-1}$ Collagenase (Worthington Biomedical Corp.,
1071 #LS004176), $0.8U{\cdot}mL^{-1}$ Dispase (Worthington Biomedical Corp., #LS02109), and $0.5mg{\cdot}mL^{-1}$
1072 DNase (Worthington Biomedical Corp., #LS006344) in 1x Hanks' Balanced Salt Solution
1073 (HBSS) with Ca^{2+} and Mg^{2+} (Gibco, # 14065056) at 37°C for 30 min on a rotating mixer. Cells
1074 were then washed with Sort Buffer and passed through a 40μm cell strainer.

1075

1076 **Endothelial cell transplantation experiments**

1077 Four days prior to transplant, recipient mice received one dose of 5-FU ($150\ mg{\cdot}kg^{-1}$ in PBS,
1078 Sigma-Aldrich, #F6627) intraperitoneally under isoflurane anesthesia. Sorted bone marrow cells
1079 (Col1a2-Cre/ZsGreen: 5,000 cells; Cdh5-Cre/ZsGreen: 20,000 cells in 100μL PBS) were
1080 inoculated retro-orbitally under isoflurane anesthesia. Bone marrows and blood were harvested
1081 from transplant recipients four weeks after the transplant unless otherwise specified.

1082

1083 **Bone marrow ablation and transplantation**

1084 Recipient mice were lethally irradiated (11 Gy) using a Cesium-137 (^{137}Cs) gamma irradiator

1085 three days prior to transplantation.

1086 For whole BM cell transplantation into *mTmG* recipients, BM cells were harvested from WT

1087 donor mice by flushing (as described above); 5×10^6 cells were transplanted per recipient via tail

1088 vein.

1089 For LSK transplantation into WT recipients, BM from Cdh5-Cre^{ERT2}(PAC)/ZsGreen mice (not

1090 treated with tamoxifen) was harvested by flushing, followed by red blood cell lysis with ACK

1091 buffer. Fc receptor blocking was performed using Azide-Free Fc Receptor Blocker (Innovex,

1092 #NB335-60) per manufacturer's instructions. Cells were stained with antibodies to Lineage

1093 cocktail, Sca-1, and c-Kit. DAPI was used to exclude dead cells. LSK populations were sorted

1094 using Sony SH800S and its Ultra Purity mode. Transplanted cell numbers were as follows:

1095 ZsGreen$^-$ LSKs (5×10^4, n = 3; 2.5×10^4, n = 3) and ZsGreen$^+$-enriched LSKs (2,800 cells, n =

1096 2).

1097 For transplantation of ex vivo–cultured BM cells, non-adherent and loosely adherent ZsGreen$^+$

1098 cells were collected from 8-week OP9 co-cultures (as described above), sorted by FACS for live

1099 (DAPI$^-$) ZsGreen$^+$ cells, and transplanted into irradiated recipients at 5×10^4, 2.5×10^4, or $1.25 \times$

1100 10^4 cells per mouse (n = 2 per group).

1101

1102 **Flow cytometry and cell sorting**

1103 For intracellular antigen detection, single cell suspensions of bone marrow and blood were first

1104 incubated with Azide-Free Fc Receptor Blocker (Innovex, #NB335-60), following the

1105 manufacturer's instructions. After washing, cells were first stained with surface marker
1106 antibodies at the concentration of 2μg per 1×10^7 cells in Sort Buffer for 30 minutes at 4°C and
1107 then stained with live/dead cell discriminating BioLegend Zombie Dyes (UV, NIR, Violet, or
1108 Yellow, BioLegend #423108, #423106, #423114, and # 423104) following the manufacturer's
1109 instructions. After washing, cells were fixed in 4% paraformaldehyde for 10 minutes at 37°C,
1110 and then permeabilized with 1% saponin (Sigma-Aldrich, # 47036) /Sort Buffer for 30min on
1111 ice. Subsequently, the cells were stained with rat monoclonal primary RUNX1-PE Ab
1112 (Invitrogen, # 12-9816-80) in 0.1% saponin/Sort Buffer overnight. After washing and
1113 resuspension, propidium iodide (PI, 0.5μM, Millipore Sigma, # P4170), 7-AAD ($1\mu g\cdot mL^{-1}$,
1114 Millipore Sigma, #A9400) or DAPI ($0.5\mu g\cdot mL^{-1}$, BioLegend, #422801) was added as a nuclear
1115 counterstain. For live cell staining without cell permeabilization, after cell surface antibody
1116 staining, cells were washed and suspended in Sort buffer containing propidium iodide (PI,
1117 0.5μM, Millipore Sigma, # P4170), 7-AAD ($1\mu g\cdot mL^{-1}$, Millipore Sigma, #A9400) or DAPI
1118 ($0.5\mu g\cdot mL^{-1}$, BioLegend, # 422801), to distinguish dead cells from the live cells. For FACS
1119 sorting of live endothelial cells, after Fc receptor blocking, bone marrow cells were first depleted
1120 of $CD45^+$ cells with MojoSort mouse CD45 nanobeads (BioLegend #480028) following the
1121 manufacturer's protocol and then stained with specific antibodies. For flow cytometry analysis,
1122 compensation beads (BD Biosciences, #552844) were used for flow cytometer compensation.
1123 Flow cytometric data were acquired with BD FACSCanto-II, BD LSRFortessa, BD
1124 FACSymphony A5 (BD Biosciences), Sony SA3800 or Sony ID7000 cell analyzers. Cell sorting
1125 was performed with BD FACS Aria III, BD FACS Aria Fusion or Sony SH800S cell sorters.
1126 FSC and SSC profiles were used for excluding dead cells and debris. 7-AAD, PI, DAPI or
1127 BioLegend Zombie Dye was used for excluding dead cells. FSC-W versus FSC-H and SSC-W

1128 versus SSC-H were used to gate on single cells. Unless otherwise specified, fluorescence minus
1129 one (FMO) controls are used for negative gating reference. For BM HSPC analysis, BM cells
1130 were harvested followed by lineage positive cell depletion (Biolegend #480004). Data were
1131 analyzed with FlowJo (BD, v10.8.1), SONY ID7000 Software (Version 1.2.0.28212) or FACS
1132 Diva (BD, v6.1 and v9.0). Flowjo Plugins UMAP_R (v4.0.4) and FlowSOM (v4.1.0) were used
1133 for UMAP dimensional reduction and unsupervised clustering of flow cytometry data.
1134
1135 **Bone marrow cryosections**
1136 Deeply anesthetized mice were transcardially perfused with 20mL ice-cold 1x PBS, followed by
1137 perfusion with 15mL ice-cold hydrogel solution (5% acrylamide/bis-acrylamide 19:1 (Sigma-
1138 Aldrich, #A2917), 2.5mg/mL polymerization initiator VA-044 (FUJIFILM, Wako, VA-044,
1139 Water soluble Azo initiators), 4% PFA in 1× PBS, 5mL/min flow speed). Femurs and tibiae were
1140 collected in tubes containing 5mL hydrogel solution and incubated at 4°C for 4 hours. The bones
1141 were then washed with PBS and incubated at 37°C for 2 hours. Bone decalcification was
1142 performed by incubating the bones in 40mL 0.5M EDTA pH 8.0 (KD Medical, #RGF-3130) for
1143 3 days on a rotate mixer, with daily refreshed 0.5M EDTA solution. The bones were then
1144 dehydrated in 20% sucrose and 2% polyvinylpyrrolidone in PBS overnight. Dehydrated bones
1145 were then embedded in OCT (SAKURA, #4583) blocks using Precision Cryoembedding System
1146 (IHC WORLD, #IW-P101). Cryosections (10μm) for immunofluorescence staining were
1147 prepared from OCT frozen bone blocks using Leica CM3050S microtome, low-profile
1148 microtome blades (Leica 819, #14035838925), and TruBond™ 380 adhesion slides (Electron
1149 Microscopy Sciences, # 63701-W10).
1150

1151 **Immunofluorescence staining and imaging**

1152 Tissue sections were rehydrated with 1× PBS (15 minutes), permeabilized in 0.3% Triton X-100
1153 (Sigma-Aldrich, #T9284)/PBS (15 minutes), washed in 1× PBS, and incubated (2 hours) with
1154 blocking solution (2% BSA, 5% donkey serum (SIGMA, #D9663), and 0.3% Triton X-
1155 100/PBS). Samples were then washed 3 times with PBS and incubated with primary antibodies
1156 (5ng/mL; 4°C overnight). When secondary antibodies were used, 3 PBS washes were performed
1157 before incubating with fluorescent-labeled secondary antibodies (2ng/mL, room temperature, 2
1158 hours). After washing (3x, 10 minutes each with 1× PBS), DAPI was added (300nM in PBS, 10
1159 min). After 3 washes (5 min each with 1× PBS), coverslips were mounted (EPREDIA,
1160 #9990402), dried and sealed with nail polish. For blood smear staining, slides were first soaked
1161 in acetone/methanol/PFA (19:19:2 for 90 seconds) before rehydration [88]. Confocal imaging was
1162 performed with Zeiss LSM 780, Zeiss LSM 880 NLO Two Photon, or Nikon *ECLIPSE* Ti2-E
1163 SoRa systems, according to the experimental specific needs (resolution, speed, wavelength
1164 capabilities). Images were processed with Zen (Zen Black v2.3, release Version 14.0.12.201, Zen
1165 Blue Lite v2.5, Carl Zeiss), Bitplane Imaris (v9.7.0, Oxford instruments), and Photoshop
1166 (v23.3.0, Adobe, for whole image contrast and brightness adjustments).

1167

1168 **Isolation of peritoneal cavity cells**

1169 To isolate peritoneal cavity cells, mice were euthanized by cervical dislocation, injected
1170 intraperitoneally (i.p.) with cold FACS sort buffer (5 mL), massaged and flicked gently on the
1171 abdomen. Peritoneal fluid was then withdrawn slowly and transferred into a polypropylene
1172 centrifuge tube on ice prior to centrifugation (350×g, 10min, at 4°C) and analysis.

1173

1174 **Thioglycolate induced sterile peritonitis**

1175 Mice were injected i.p. with 1 mL PBS or 4% thioglycolate (Sigma-Aldrich, #70157). Peritoneal
1176 cavity cells were harvested 4 hours after injection for further analysis.

1177

1178 **Phagocytosis assay**

1179 Phagocytosis assay was performed using pHrodo™ Red *Escherichia coli* BioParticles
1180 (Invitrogen, # P35361) following the manufacturer's instructions. Briefly, mice were first treated
1181 with thioglycolate (as described). Peritoneal cavity cells were incubated with the fluorescent
1182 *Escherichia coli* particles for 60 min at 37°C. Cells were then stained with surface marker
1183 antibodies and analyzed by flow cytometry.

1184

1185 **ROS assay**

1186 ROS assay was performed using CellROX™ Orange Flow Cytometry Assay Kit (Invitrogen, #
1187 C10493) following the manufacturer's instructions. Briefly, mice were first treated with
1188 thioglycolate (as described). CellROX detection reagent was added to peritoneal cavity cells
1189 (final concentration of 500nM) prior to incubation for 60 min at 37°C. Cells were then stained
1190 with the surface marker antibodies and analyzed by flow cytometry.

1191

1192 **PolyloxExpress single cell lineage tracing**

1193 These experiments essentially followed published procedures [33]. Briefly, BM cells from
1194 tamoxifen treated Cdh5-Cre/ZsGreen/Polylox mice (treated at 10 weeks old and harvested at 16
1195 weeks old) were enriched for ZsGreen positive cells by FACS. Single cell capturing was
1196 performed with 10x Genomics Chromium Single Cell 3′ Reagent Kits, following manufacturer's

1197 protocols. After reverse transcription (RT) in droplets, pooled cDNA was amplified and split into
1198 two aliquots for parallel transcriptome library preparation and barcode enrichment. Initial library
1199 quality control was performed with Agilent TapeStation D5000. For transcriptome analysis, 10
1200 µL (25%) of a 10x cDNA library was fragmented and a gene expression library, generated
1201 following protocols in Single Cell 3' Reagent Kits v3 and v4, was sequenced with Illumina
1202 NextSeq 2000 P3/P4 Reagents (28+74 bp read length). For Polylox barcode amplification,
1203 targeted amplification of barcodes from a 5-10 ng aliquot of a 10x cDNA library was performed
1204 by nested PCR. In the first round, primers #2,652 (5′-GCATGGACGAGCTGTACAAG-3′,
1205 annealing at the 5′ end of Polylox) and #2,674 (5′-
1206 AATGATACGGCGACCACCGAGATCTACACTCTTTCCCTACACGACGCTC-3′, annealing
1207 at the adaptor site (read 1) were used for amplification for 5 min at 95°C; (30 s at 95°C, 30 s at
1208 57°C, 3 min at 72°C) 12 times; 10 min at 72°C. PCR products purified with 0.7x AMPure beads
1209 were used for the second round of PCR using primers #2,426 (5′-
1210 CGACGACACTGCCAAAGATTTC-3′, annealing at the 5′ end of Polylox) and #2,676 (5′-
1211 AATGATACGGCGACCACCGA-3′, annealing at the 5′ end of primer #2,674), for 5 min at
1212 95°C; (30 s at 95°C, 30 s at 60°C, 3 min at 72°C) 18 times; 10 min at 72°C. The PCR products
1213 were purified with AMPure PB beads according to the manufacturer's protocol. Long read
1214 amplicon-seq libraries were sequenced by PacBio Sequel II with PacBio Amplicons Library
1215 Preparation using SMRTbell prep kit 3.0. A custom transcriptome reference was built from
1216 mouse reference MM10 to include ZsGreen1.
1217 A snakemake workflow with custom python script was used to retrieve cell indexes and Polylox
1218 barcodes from the PolyloxExpress amplicons (https://github.com/CCRSF-IFX/SF_Polylox-BC).
1219 Single cell transcriptome and single cell barcodes were linked using the 10x 3' kit cell index and

1220 group information. Further analysis and illustrations were generated using Scanpy
1221 (https://github.com/scverse/scanpy). Doublet detection was performed using Scrublet, with the
1222 predicted doublet rate calculated based on 10x Genomics guidance about the cell numbers loaded
1223 to the microfluidic chips. Batch correction was done using BBKNN method
1224 (https://github.com/Teichlab/bbknn). Cell types were manually annotated based on canonical
1225 marker gene expression, guided by results from three automated annotation tools: (1) decoupleR
1226 ((https://saezlab.github.io/decoupleR/), using PangLaoDB (https://panglaodb.se/) as reference;
1227 (2) scANVI (https://github.com/scverse/scvi-tools) using ImmGne (https://www.immgen.org/) as
1228 reference; (3) CellTypist, using the embedded Immune_All_Low model. The rare barcodes and
1229 their pGen were identified using the MatLab script from the Höefer's Lab
1230 (https://github.com/hoefer-lab/polylox). True barcodes are defined as pGen < 1×10^{-4}, such that
1231 the expectation of a True barcode in detected 4,072 cells is 0.407. This work utilized the
1232 computational resources of the NIH HPC Biowulf cluster (*http://hpc.nih.gov*) and Frederick
1233 Research Computing Environment (FRCE). Python version: 3.10.; R version 4.5.0.
1234

1235 **Public single-cell RNA-seq data analysis**

1236 Raw FASTQ and BAM files were downloaded from publicly available datasets (GSE108885 [54],
1237 GSE108891 [54], GSE118436 [54], GSE123078 [54], GSE122465 [55], GSE128423 [53], GSE145477 [65],
1238 GSE156635 [56], GSE137116 [24], E-MTAB-8077 [65], GSE230260[58], GSE259382[59]). The BAM files
1239 were first converted to FASTQ files with bamtofastq (10x Genomics, v2.0.1). All FASTQ files
1240 were then processed by the count function of Cell Ranger (10x Genomics, v8.0.1) and aligned to
1241 the mouse genome (mm10, version 2020-A), to generate read matrixes. Further analysis and
1242 illustrations were generated using Scanpy as described above.

1243

1244 **Definition of cultured fluorescent BM cell clusters and quantification**

1245 A cluster was defined as (1) a spatially distinct group of ZsGreen^{+} cells not contiguous with other
1246 fluorescent cells, (2) containing a central core with at least five extending branches, and (3)
1247 exhibiting a roughly radial organization, with projections spreading outward in multiple
1248 directions, and (4) extending at least ~200 µm in one direction. Isolated or irregularly scattered
1249 fluorescent cells were not counted. Due to their large size, clusters were counted manually across
1250 the culture dish using a tally counter under fluorescence microscopy.

1251

1252 **RNA isolation and quantitative RT PCR**

1253 RNA was extracted using RNeasy® Micro Kit (QIAGEN, #74004), following the manufacturer's
1254 protocol. Cells were sorted directly into RNA lysis buffer (Buffer RTL of RNeasy® Micro Kit).
1255 cDNA samples were prepared with SuperScript IV Reverse Transcriptase (Invitrogen,
1256 #18091050), following manufacturer's instructions. Real Time PCR was performed using
1257 Applied Biosystems™ TaqMan™ Fast Advanced Master Mix (4444557) and Applied
1258 Biosystem™ QuantStudio™ 5 Real-Time PCR System. TaqMan™ probes used were purchased
1259 from Applied Biosystems™: Spp1 (Mm00436767_m1); Cxcl12 (Mm00445553_m1); Col1a2
1260 (Mm00483888_m1); Cdh5 (Mm00486938_m1); Runx1 (Mm01213404_m1); Ptprc
1261 (Mm01293577_m1); Gapdh (Mm99999915_g1); Actb (Mm02619580_g1). The reaction
1262 condition was set as follows: 50°C 2 minutes, 95°C 20 seconds, 45 cycles of 95°C 1 second,
1263 60°C 20 seconds. Ct values were determined using the ABI QuantStudio™ Design & Analysis
1264 Software (v1.5.2). Relative gene expression was assessed using the $2^{-\Delta\Delta Ct}$ method, normalized to
1265 Gapdh expression level for each sample. The data was further normalized to gene expression

levels in the unsorted bone marrow sample to calculate relative gene expression levels in each sample. Data reflect triplicates real-time PRC experiments.

QUANTIFICATION AND STATISTICAL ANALYSIS

No statistical method was used to predetermine sample size. No data were excluded from the analyses. Mice with the correct genotypes were randomly assigned to control or treated groups. Unless otherwise specified, data are represented as mean ± S.D, and individual dots in the graphs indicate individual mice. Comparisons between two groups were performed using two-tailed unpaired Student's *t*-tests (except for Figure S1-H, which used a paired *t*-test). Spearman rank correlation test was used for Figure 3E. Statistical analyses were performed with GraphPad Prism (v9.0.1). A statistical difference of $P<0.05$ was considered significant: ns, not significant, * $P < 0.05$, ** $P < 0.01$, *** $P< 0.001$.

Figure 1

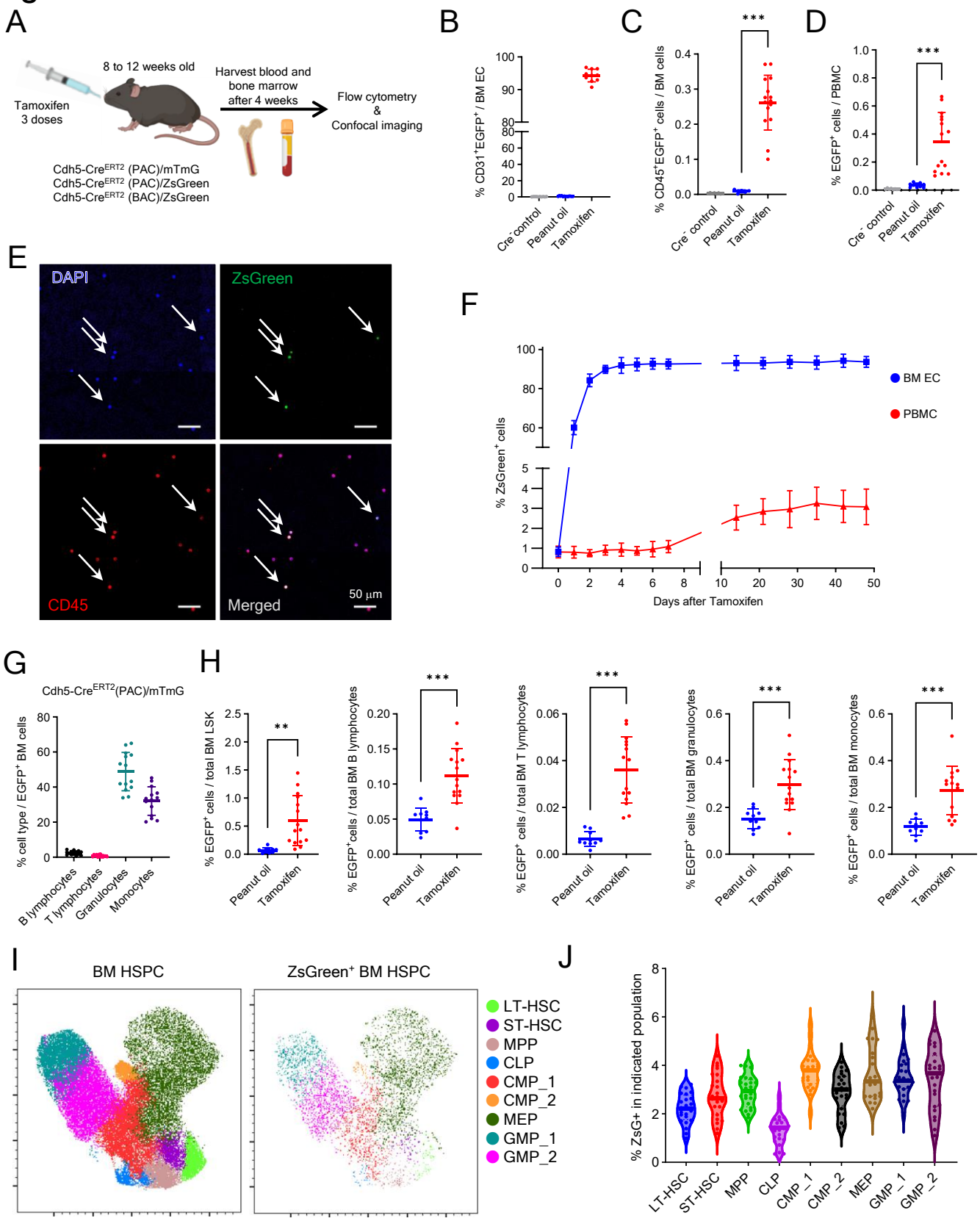
A
8 to 12 weeks old
Tamoxifen
3 doses
Harvest blood and
bone marrow
after 4 weeks
Flow cytometry
&
Confocal imaging
Cdh5-CreERT2 (PAC)/mTmG
Cdh5-CreERT2 (PAC)/ZsGreen
Cdh5-CreERT2 (BAC)/ZsGreen
B
% CD31+EGFP+ / BM EC
Cre- control
Peanut oil
Tamoxifen
C
% CD45+EGFP+ cells / BM cells
***
D
% EGFP+ cells / PBMC
***
E
DAPI
ZsGreen
CD45
Merged
50 µm
F
% ZsGreen+ cells
BM EC
PBMC
Days after Tamoxifen
G
Cdh5-CreERT2(PAC)/mTmG
% cell type / EGFP+ BM cells
B lymphocytes
T lymphocytes
Granulocytes
Monocytes
H
% EGFP+ cells / total BM LSK
**
% EGFP+cells / total BM B lymphocytes
% EGFP+ cells / total BM T lymphocytes
% EGFP+ cells / total BM granulocytes
% EGFP+ cells / total BM monocytes
Peanut oil
Tamoxifen
I
BM HSPC
ZsGreen+ BM HSPC
LT-HSC
ST-HSC
MPP
CLP
CMP_1
CMP_2
MEP
GMP_1
GMP_2
J
% ZsG+ in indicated population
LT-HSC
ST-HSC
MPP
CLP
CMP_1
CMP_2
MEP
GMP_1
GMP_2

Figure 2

A

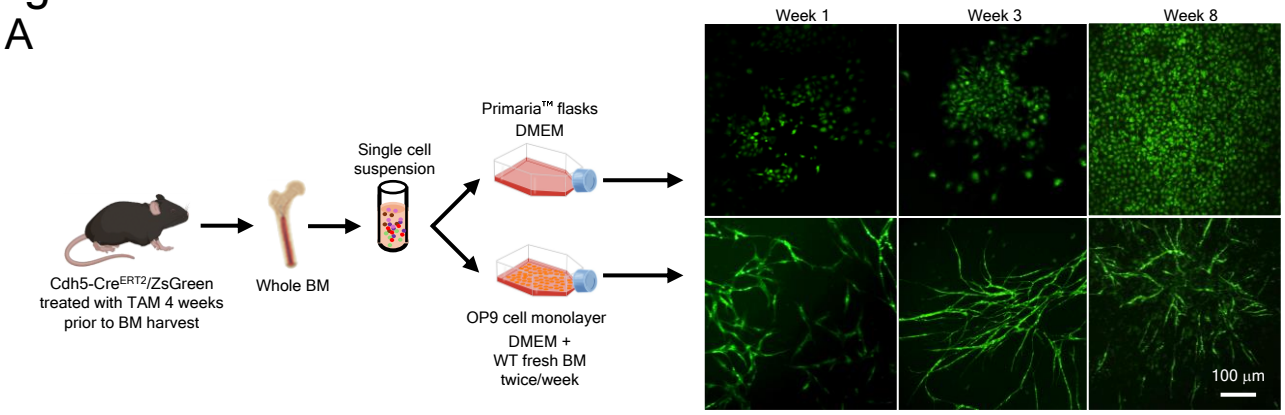

B

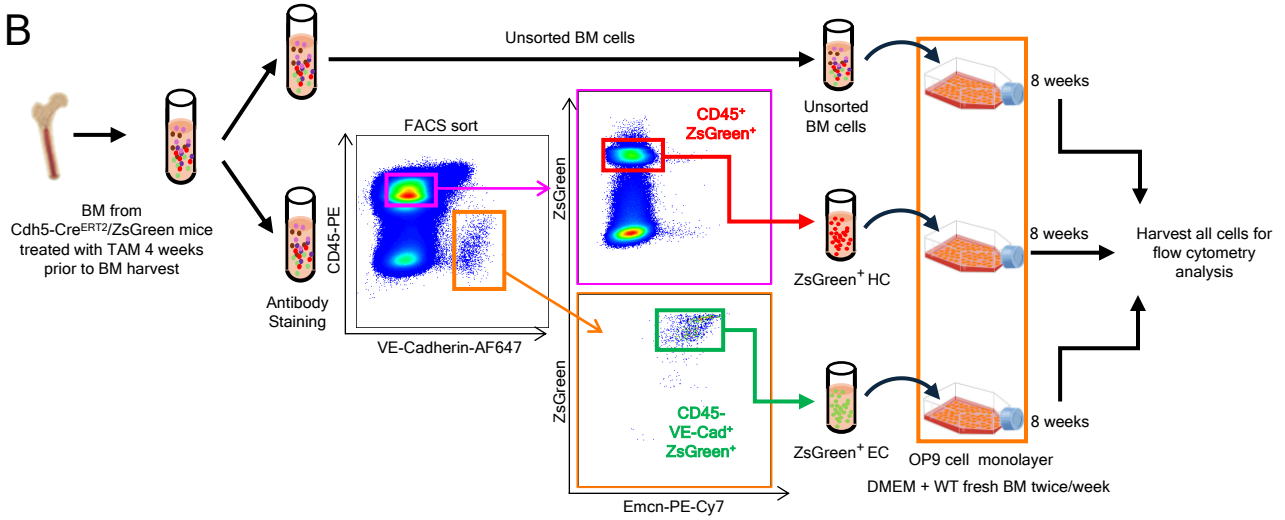

C

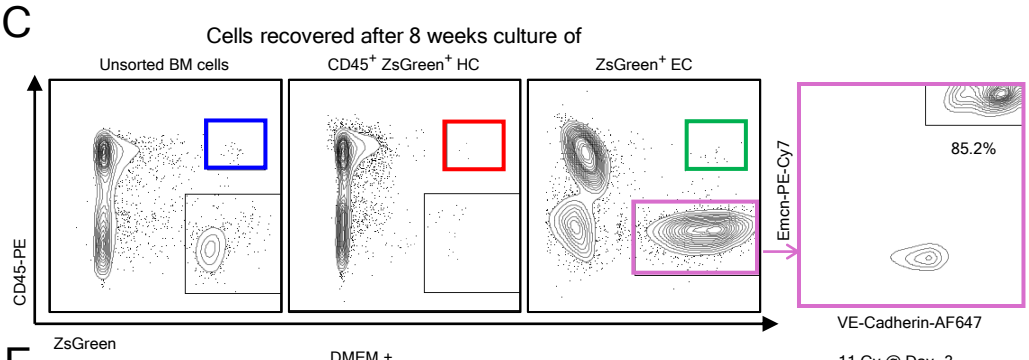

D

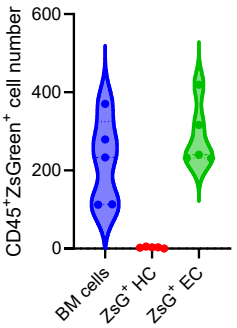

E

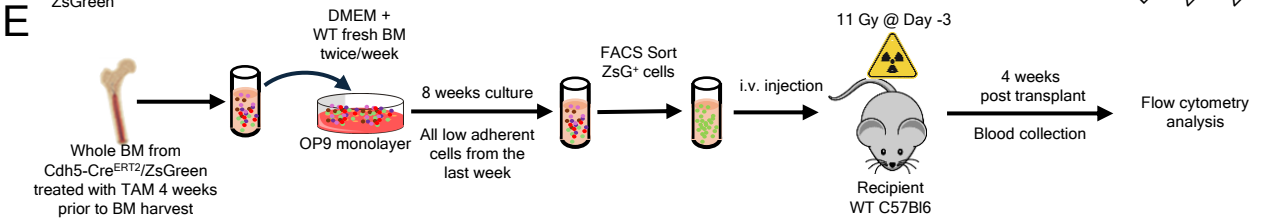

F

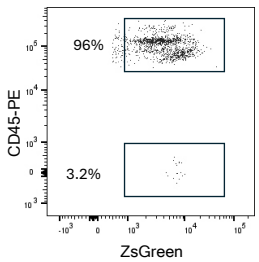

G

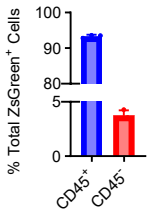

H

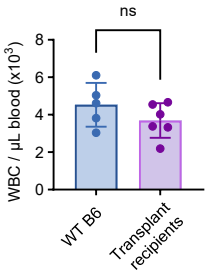

I

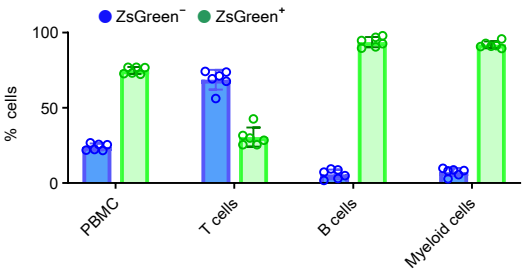

Figure 3

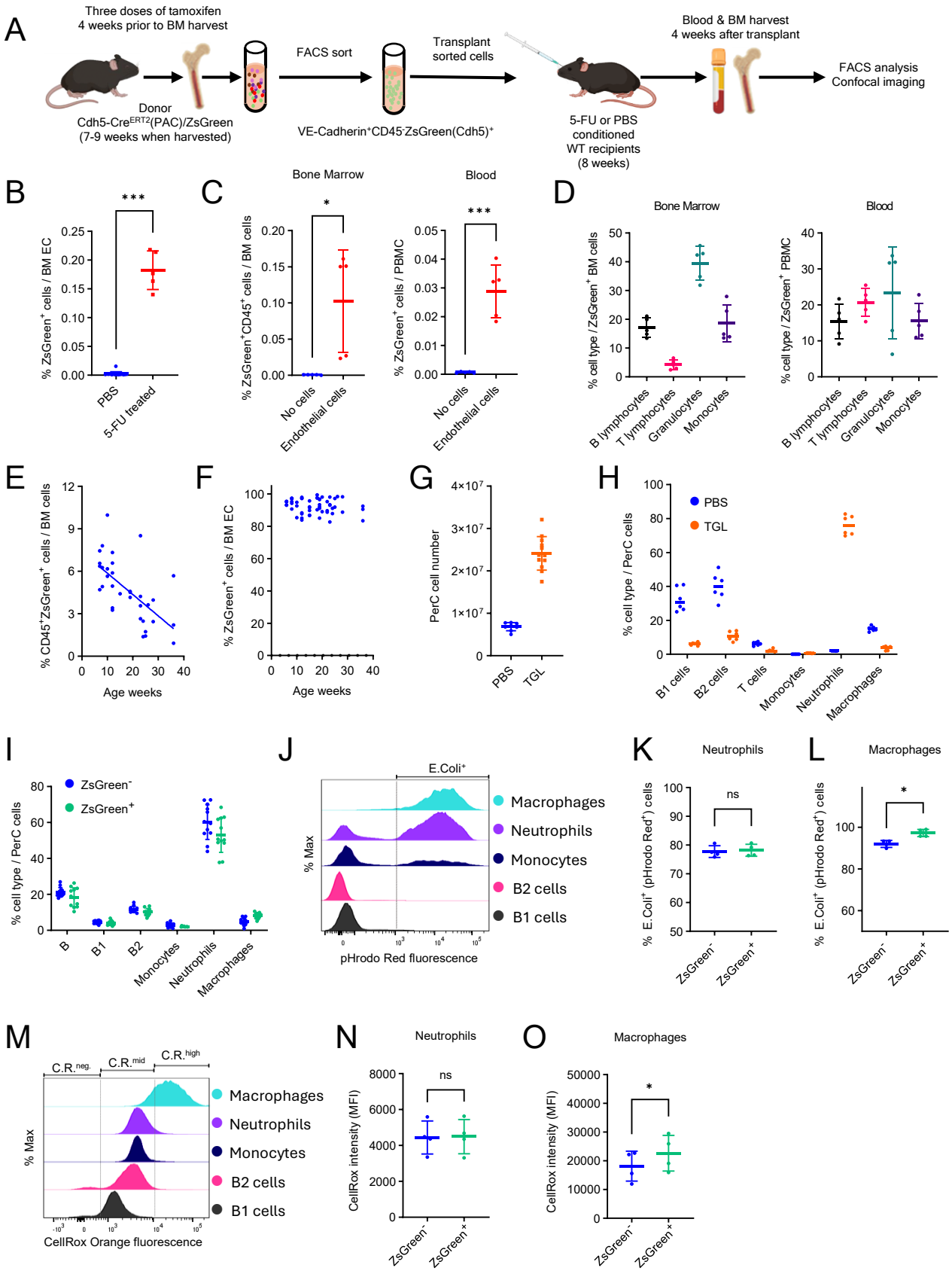
A
Three doses of tamoxifen
4 weeks prior to BM harvest
Donor
Cdh5-CreERT2(PAC)/ZsGreen
(7-9 weeks when harvested)
FACS sort
VE-Cadherin+CD45-ZsGreen(Cdh5)+
Transplant
sorted cells
5-FU or PBS
conditioned
WT recipients
(8 weeks)
Blood & BM harvest
4 weeks after transplant
FACS analysis
Confocal imaging
B
% ZsGreen+ cells / BM EC
PBS
5-FU treated
C
Bone Marrow
Blood
% ZsGreen+CD45+ cells / BM cells
No cells
Endothelial cells
% ZsGreen+ cells / PBMC
D
Bone Marrow
Blood
% cell type / ZsGreen+ BM cells
% cell type / ZsGreen+ PBMC
B lymphocytes
T lymphocytes
Granulocytes
Monocytes
E
% CD45+ZsGreen+ cells / BM cells
Age weeks
F
% ZsGreen+ cells / BM EC
Age weeks
G
PerC cell number
PBS
TGL
H
PBS
TGL
% cell type / PerC cells
B1 cells
B2 cells
T cells
Monocytes
Neutrophils
Macrophages
I
ZsGreen-
ZsGreen+
% cell type / PerC cells
B
B1
B2
Monocytes
Neutrophils
Macrophages
J
E.Coli+
% Max
Macrophages
Neutrophils
Monocytes
B2 cells
B1 cells
pHrodo Red fluorescence
K
Neutrophils
ns
% E.Coli+ (pHrodo Red+) cells
ZsGreen-
ZsGreen+
L
Macrophages
*
% E.Coli+ (pHrodo Red+) cells
ZsGreen-
ZsGreen+
M
C.R.neg.
C.R.mid
C.R.high
% Max
Macrophages
Neutrophils
Monocytes
B2 cells
B1 cells
CellRox Orange fluorescence
N
Neutrophils
ns
CellRox intensity (MFI)
ZsGreen-
ZsGreen+
O
Macrophages
*
CellRox intensity (MFI)
ZsGreen-
ZsGreen+

Figure 4

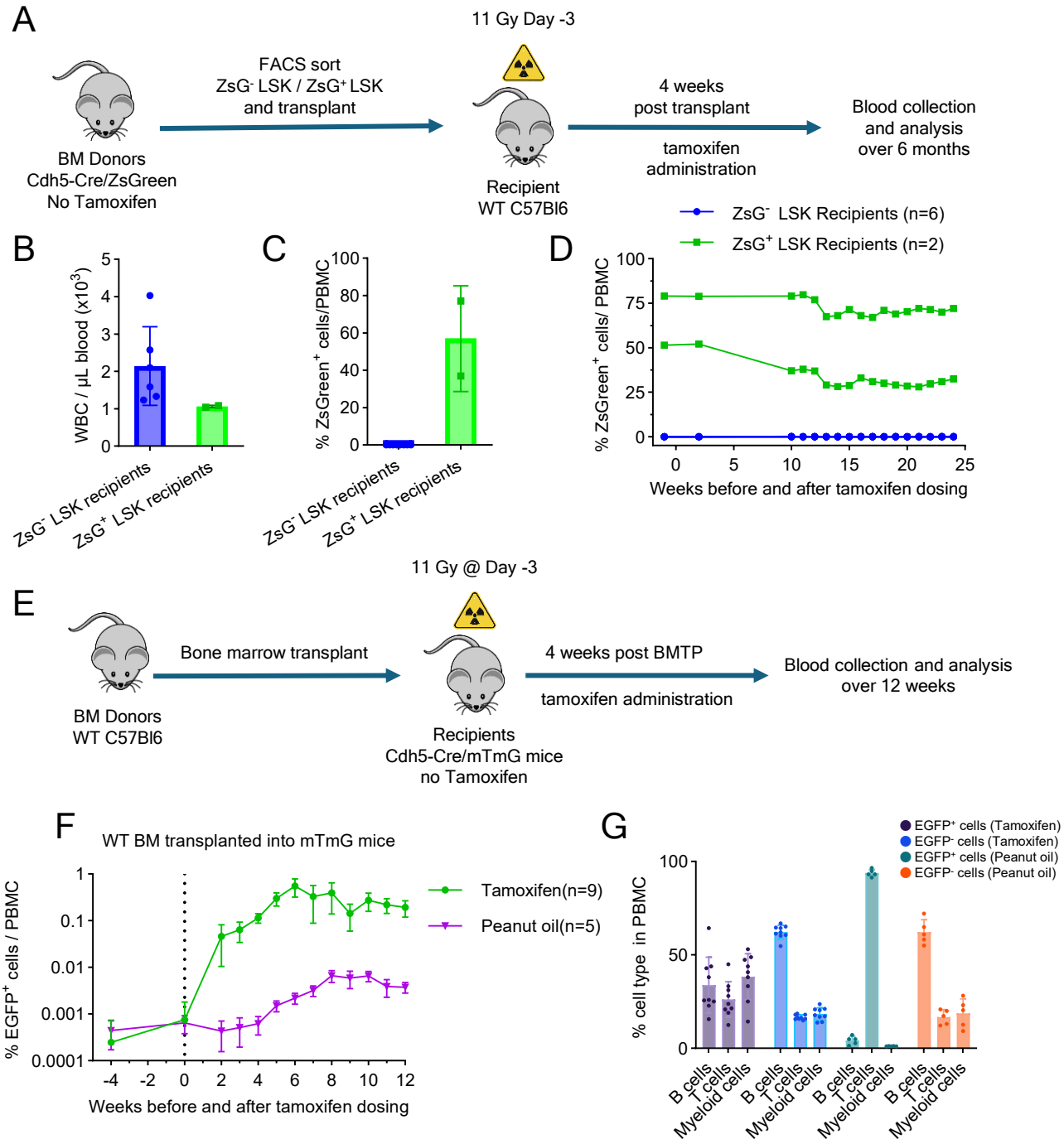
A
11 Gy Day -3
FACS sort
ZsG- LSK / ZsG+ LSK
and transplant
BM Donors
Cdh5-Cre/ZsGreen
No Tamoxifen
Recipient
WT C57Bl6
4 weeks
post transplant
tamoxifen
administration
Blood collection
and analysis
over 6 months
B
WBC / µL blood (x10^3)
ZsG- LSK recipients
ZsG+ LSK recipients
C
% ZsGreen+ cells/PBMC
ZsG- LSK recipients
ZsG+ LSK recipients
D
ZsG- LSK Recipients (n=6)
ZsG+ LSK Recipients (n=2)
% ZsGreen+ cells/ PBMC
Weeks before and after tamoxifen dosing
11 Gy @ Day -3
E
Bone marrow transplant
BM Donors
WT C57Bl6
Recipients
Cdh5-Cre/mTmG mice
no Tamoxifen
4 weeks post BMTP
tamoxifen administration
Blood collection and analysis
over 12 weeks
F
WT BM transplanted into mTmG mice
% EGFP+ cells / PBMC
Tamoxifen(n=9)
Peanut oil(n=5)
Weeks before and after tamoxifen dosing
G
EGFP+ cells (Tamoxifen)
EGFP- cells (Tamoxifen)
EGFP+ cells (Peanut oil)
EGFP- cells (Peanut oil)
% cell type in PBMC
B cells
T cells
Myeloid cells

Figure 5

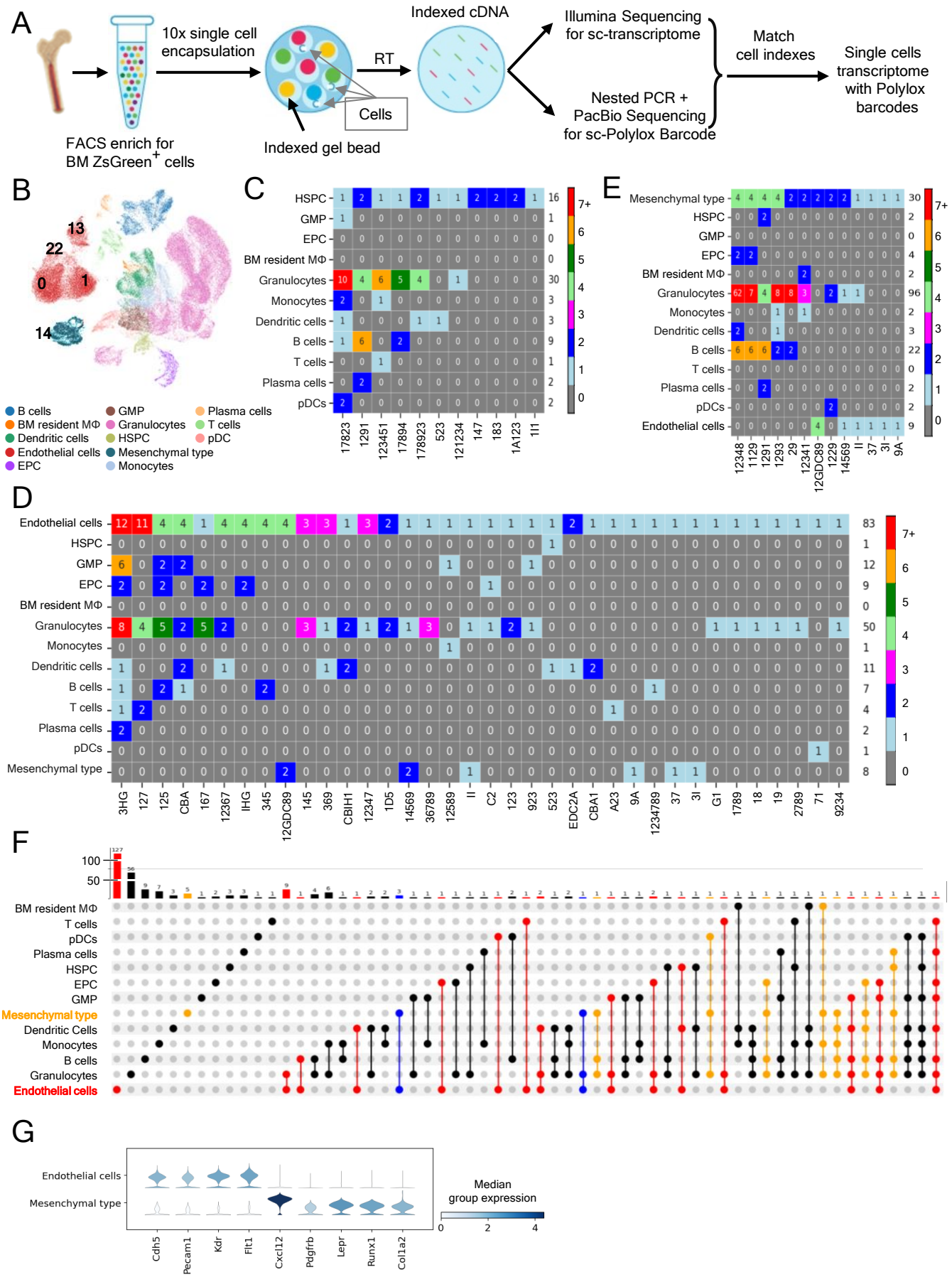
A
10x single cell encapsulation
FACS enrich for BM ZsGreen+ cells
Indexed gel bead
Cells
RT
Indexed cDNA
Illumina Sequencing for sc-transcriptome
Nested PCR + PacBio Sequencing for sc-Polylox Barcode
Match cell indexes
Single cells transcriptome with Polylox barcodes
B
13
22
0
1
14
B cells
BM resident MΦ
Dendritic cells
Endothelial cells
EPC
GMP
Granulocytes
HSPC
Mesenchymal type
Monocytes
Plasma cells
T cells
pDC
C
HSPC
GMP
EPC
BM resident MΦ
Granulocytes
Monocytes
Dendritic cells
B cells
T cells
Plasma cells
pDCs
17823 1291 123451 17894 178923 523 121234 147 183 1A123 1I1
E
Mesenchymal type
HSPC
GMP
EPC
BM resident MΦ
Granulocytes
Monocytes
Dendritic cells
B cells
T cells
Plasma cells
pDCs
Endothelial cells
12348 1129 1291 1293 29 12341 12GDC89 1229 14569 1I 37 3I 9A
D
Endothelial cells
HSPC
GMP
EPC
BM resident MΦ
Granulocytes
Monocytes
Dendritic cells
B cells
T cells
Plasma cells
pDCs
Mesenchymal type
3HG 127 125 CBA 167 12367 IHG 345 12GDC89 145 369 CBIH1 12347 1D5 14569 36789 12589 1I C2 123 923 523 EDC2A CBA1 A23 9A 1234789 37 3I G1 1789 18 19 2789 71 9234
F
BM resident MΦ
T cells
pDCs
Plasma cells
HSPC
EPC
GMP
Mesenchymal type
Dendritic Cells
Monocytes
B cells
Granulocytes
Endothelial cells
G
Endothelial cells
Mesenchymal type
Cdh5 Pecam1 Kdr Flt1 Cxcl12 Pdgfrb Lepr Runx1 Col1a2
Median group expression
0 2 4

Figure 6

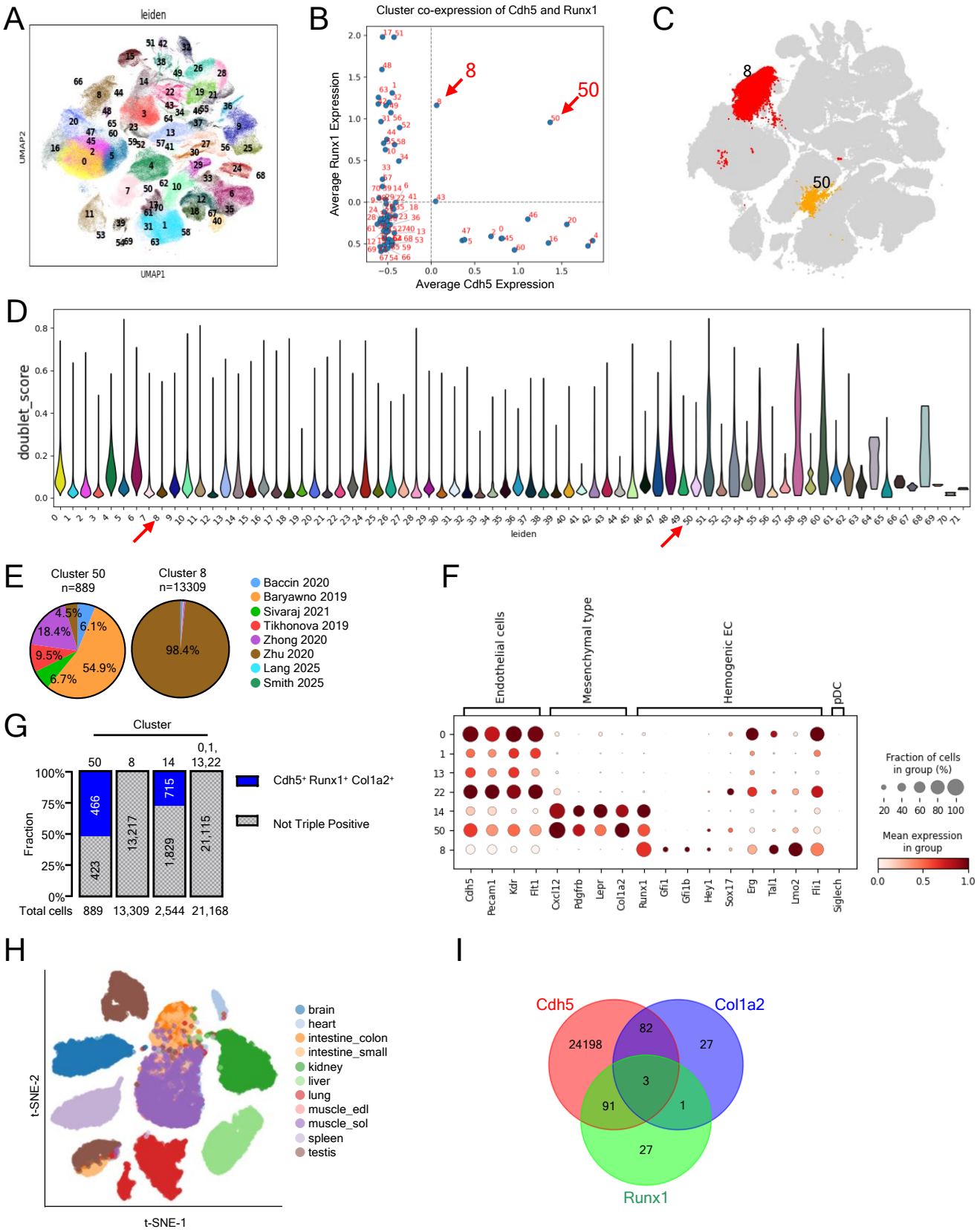
A
leiden
UMAP2
UMAP1
B
Cluster co-expression of Cdh5 and Runx1
Average Runx1 Expression
Average Cdh5 Expression
8
50
C
8
50
D
doublet_score
leiden
E
Cluster 50
n=889
Cluster 8
n=13309
4.5%
6.1%
18.4%
9.5%
54.9%
6.7%
98.4%
Baccin 2020
Baryawno 2019
Sivaraj 2021
Tikhonova 2019
Zhong 2020
Zhu 2020
Lang 2025
Smith 2025
F
Endothelial cells
Mesenchymal type
Hemogenic EC
pDC
Cdh5
Pecam1
Kdr
Flt1
Cxcl12
Pdgfrb
Lepr
Col1a2
Runx1
Gfi1
Gfi1b
Hey1
Sox17
Erg
Tal1
Lmo2
Fli1
Siglech
Fraction of cells in group (%)
Mean expression in group
G
Cluster
50
8
14
0,1, 13,22
Fraction
466
423
13,217
715
1,829
21,115
Cdh5+ Runx1+ Col1a2+
Not Triple Positive
Total cells
889
13,309
2,544
21,168
H
t-SNE-2
t-SNE-1
brain
heart
intestine_colon
intestine_small
kidney
liver
lung
muscle_edl
muscle_sol
spleen
testis
I
Cdh5
Col1a2
Runx1
24198
82
27
3
91
1
27

Figure 7

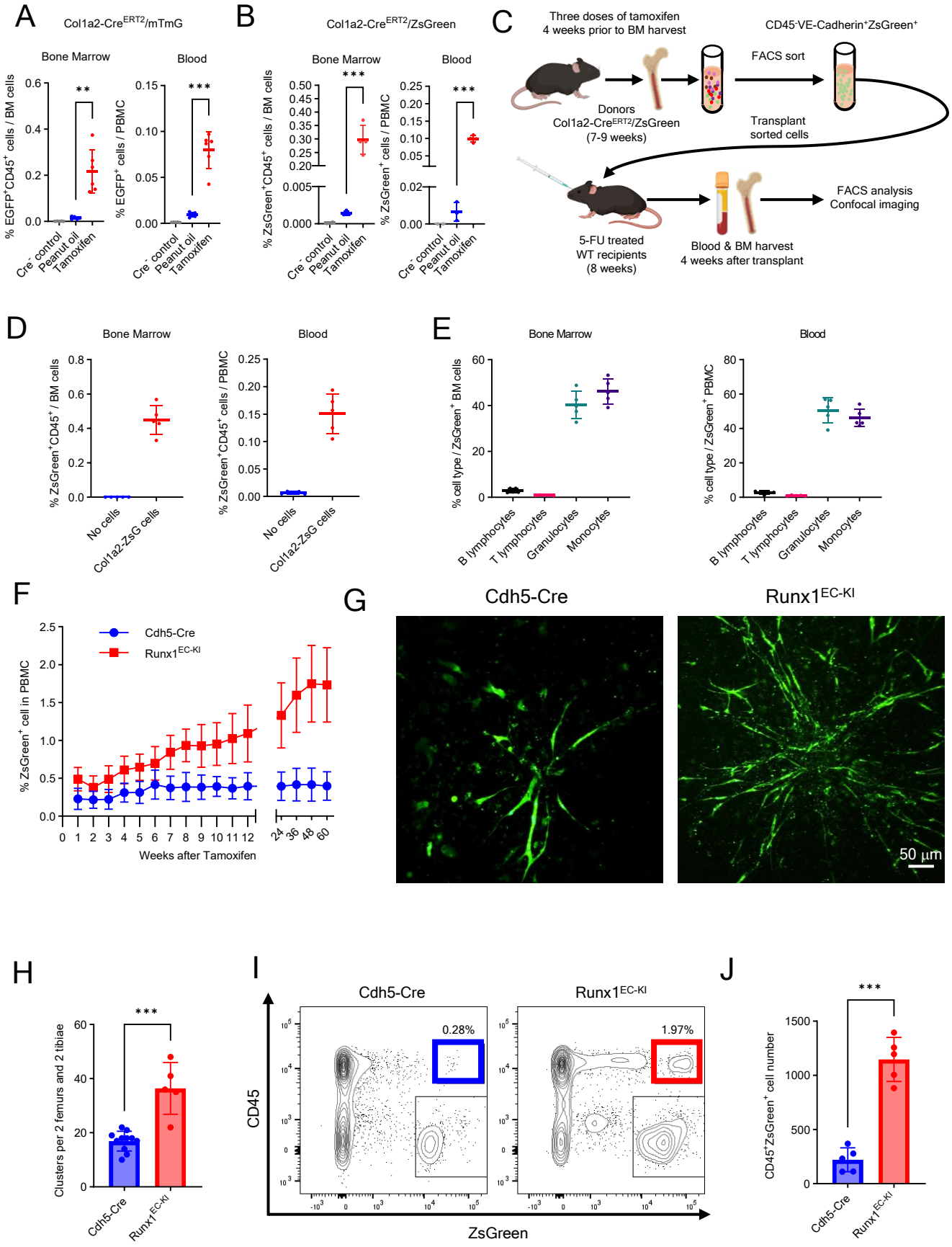
A
Col1a2-CreERT2/mTmG
Bone Marrow
Blood
% EGFP+CD45+ cells / BM cells
% EGFP+ cells / PBMC
Cre- control
Peanut oil
Tamoxifen
B
Col1a2-CreERT2/ZsGreen
% ZsGreen+CD45+ cells / BM cells
% ZsGreen+ cells / PBMC
C
Three doses of tamoxifen
4 weeks prior to BM harvest
CD45-VE-Cadherin+ZsGreen+
FACS sort
Donors
Col1a2-CreERT2/ZsGreen
(7-9 weeks)
Transplant
sorted cells
5-FU treated
WT recipients
(8 weeks)
Blood & BM harvest
4 weeks after transplant
FACS analysis
Confocal imaging
D
% ZsGreen+CD45+ / BM cells
% ZsGreen+CD45+ cells / PBMC
No cells
Col1a2-ZsG cells
E
% cell type / ZsGreen+ BM cells
% cell type / ZsGreen+ PBMC
B lymphocytes
T lymphocytes
Granulocytes
Monocytes
F
Cdh5-Cre
Runx1EC-KI
% ZsGreen+ cell in PBMC
Weeks after Tamoxifen
G
Cdh5-Cre
Runx1EC-KI
50 µm
H
Clusters per 2 femurs and 2 tibiae
I
Cdh5-Cre
Runx1EC-KI
0.28%
1.97%
CD45
ZsGreen
J
CD45+ZsGreen+ cell number